# Contents

Table 2 contains an overview of all symbols used in this lab report.

| Symbol | Meaning |
|---|---|
| $a$ | Active areas |
| $\mathfrak{a}$ | Measure for absorption |
| $c$ | Speed of light |
| $d$ | Distance between needle and laser |
| $D$ | Difussion constant |
| $e$ | Elementary charge |
| $\boldsymbol{E}$ | Electric field |
| $E_\mathrm{g}$ | Band gap energy |
| $h$ | Planck constant |
| $l$ | Length of the germanium sample |
| $L$ | Pyro signal without a semiconductor applied infront of |
| $m$ | Mass |
| $M$ | Counts of the background measurement |
| $N$ | Bin content of the main measurement |
| $P$ | Data point from the pyro detector |
| $R$ | Ohmic resistance |
| $\mathcal{R}$ | Energy resolution |
| $S$ | Signal from the semiconductor |
| $t$ | Time |
| $\mathfrak{t}$ | Measure for transimission |
| $U$ | Voltage |
| $\mu$ | Mobility |
| $\eta$ | Absorption ratio |
| $\kappa$ | Ambipolar carrier cloud |
| $\phi$ | Angle |
| $\psi$ | Angle |
| $\rho$ | Electrical resistance |
| $\sigma$ | Standard deviation of a Gaussian |
| $\tau$ | Mean life time |
| $\chi^2_\nu$ | reduced $\chi^2$ |
| $א, ב, ג, ד$ | Parameters of regression |
| $A, x_c, b, C$ | Fitparameter |
| $s_x$ | Uncertainty of $x$ |

Table 2: Symbols used in this lab report.

# 1 Physical Basics

## 1.1 Semiconductor

One option to characterize the electrical conductivity of a material is the specific electrical resistance $\rho$ defined as

$$\rho = R \cdot \frac{A}{l}, \tag{1}$$

where $A$ is the cross-sectional area perpendicular to the current, $l$ the length and $R$ the ohmic resistance of the material. Based on the specific electrical resistance, one can differentiate three different types of material: So called insulators are characterized by their electrical resistance of $\rho \geq 10^8\,\Omega\,\mathrm{cm}$, materials with $\rho \leq 10^{-3}\,\Omega\,\mathrm{cm}$ are called conductors. The last type is known as semiconductor whereby the electrical

resistance of semiconducting materials lies between those bounds: $10^{-3}\,\Omega\,\mathrm{cm} \leq \rho \leq 10^{8}\,\Omega\,\mathrm{cm}$.

## 1.2 Band theory

The macroscopic observation that different materials conduct electricity on various orders of magnitude can be explained by the so called band theory. This model results from quantum mechanical descriptions of the electrons of an atom: One single atom has discrete energy levels which an electron can inhibit. However, if the internuclear distance of two atoms is reduced to a magnitude of a few nano meters, the electrons of both atoms are able to interact with each other. As more energy states are allowed now, the amount of levels an electron can inhibit grows. Increasing the amounts of electrons leads to a mixing of states, forming continuous "bands". This allows a single electron to exist within an energy band outside the orbital belonging to the respective atom.

For our understanding of the behaviour of semiconductors two specific bands are of special interest: One is the so called valence band which distinguishes itself as the band with the highest range of energies in which electrons are present at absolute zero temperature. As the total angular momentum of the electrons sum up to zero, electrons in the valence band do not contribute to the electrical conductivity. The other band of interest is the conduction band; this is the energetically lowest band above the valence band where electrons are permitted to exist. Other than electrons in the valence band the electrons in the conduction band can contribute to the electrical conductivity of the material.

Using the band theory, one can explain the difference between conductors, semiconductors and isolators: These materials differ by the so called band gab energy $E_\mathrm{g}$ which is defined as the energy a valence electron has to be supplied with to change to the conduction band. This can be accomplished in several ways such as thermal energy, radiation or lattice movements. Isolators have a mostly full valence band (meaning that most of the carriers of charge inhibit the valence band) and an empty conduction band. As the band gap energy amounts to several electron volts, it is uncommon for an electron to switch bands. Semiconductors also have a completely full valence band and an empty conduction band, but the band gap energy is on a scale of a few electron volts, allowing thermal excitation of valence electrons. For conductors the valence and conductor band are wide enough to overlap. Due to this, there is no band gap energy and electrons can change between valence and conduction band without being supplied with energy.

## 1.3 Mobility of free carriers

In a semiconductor in equilibrium, the electron-hole pairing rate equals the recombination rate of electrons and holes. Each electron-hole pair has an mean life time $\tau$. If an electric field $\boldsymbol{E}$ is applied to the semiconductor, the charges act on the electric field and start to move. The mean velocity can then be descibed as

$$\boldsymbol{v}_\mathrm{n} = -\frac{e\tau}{m_\mathrm{n}}\boldsymbol{E} = -\mu_\mathrm{n}\boldsymbol{E}, \qquad \boldsymbol{v}_\mathrm{p} = \frac{e\tau}{m_\mathrm{p}}\boldsymbol{E} = \mu_\mathrm{p}\boldsymbol{E}. \tag{2}$$

$\mu_\mathrm{n}$ and $\mu_\mathrm{p}$ denote the mobility of the charge carriers and $m_\mathrm{n}$ and $m_\mathrm{p}$ the mass of the charge carriers. Additionally, the diffusion has an influence on the charge

transport, because the charge cloud diverges which is due to the interaction of the charge carriers between each other.

By defining the ambipolar charge distribution $c$ and considering the different charge carrier concentration, one can derive a differential equation for $c$:

$$\frac{\partial \kappa}{\partial t} = -\mu_e \boldsymbol{E} \cdot \boldsymbol{\nabla} \kappa + D \nabla^2 \kappa - \frac{\kappa - \kappa_0}{\tau_\mathrm{n}} \tag{3}$$

This equation is solved by

$$\kappa(t, x) = C \cdot \mathrm{e}^{\frac{t}{\tau_\mathrm{n}}} \cdot \frac{1}{\sqrt{4\pi D t}} \mathrm{e}^{-\frac{(x+\mu_e E t)^2}{4Dt}} \tag{4}$$

A detailed derivation is out of the scope of this report can be found in well-known literature [4]. In our experiment, the shape of the ambipolar charge distribution can be viewed by an oscilloscope.

## 1.4 Doping

The considerations so far have been based on perfect semiconductors without taking notice of defect of the crystall structure or contamination by other atoms in the material. Other atoms in the material can either have more valence electrons than the atoms of the semiconductor and therefore this electrons can be used as conduction electrons or have less electrons that the atoms of the semiconductor which leads to additional holes in the valence band. Atoms adding electrons are called donors and the one with less acceptors. Such atoms are getting add to semiconductors intentionally to increase their electrical conductivity. This process is called doping and semiconductors which are doped with donors are called n-type and the once doped with acceptors p-type.

## 1.5 p-n-diode

P-n diodes are build of a n-type semiconductor and a p-type semiconductor. In the boundary layer, the free electrons of the n-type semiconductor can enter the holes of the p-type semiconductor. This results in positively ionized atoms in the n-type semiconductor and negatively ionized atoms in the p-type semiconductor which in turn leads to the development of an electric field in the transition area. This area is called the depletion layer. Due to the electric field, electrons generated by thermal or photonic excitation will be forced out of the depletion layer.

The forms the basic framework for semiconductor detectors: An ionizing particle flying through the depletion layer generates free charges. These charges are forced out of the depletion layer and can then be measured as a current which is proportional to the energy of the passing particle.

# 2 Measuring the Band Gap Energy

In this part of the experiment, the band gap energies of germanium and silicon are to be determined by measuring absorption and transmission of a semiconductor sample when exposed to light of different energies.

## 2.1 Setup and Procedure

### 2.1.1 Setup

The basic setup for this experiment is shown in fig. 1. The light from a lamp mounted on a V-formed optical bank passes through a chopper: By blocking the light source with a frequency of 70 Hz, the chopper converts the continuous light beam into pulsed light packets. After passing through a focusing lens (not pictured in the figure) the light now hits a grating mounted at the center of an angle plate which again is mounted at the juncture of the optical bank. The plate can be rotated through a motor connected through a computer, allowing the angle to be measured. As the white light gets diffracted at the grating, it gets split up into a spectrum of different wavelengths. On the other end of the optical bank, an aperture and a filter are mounted in front of a semiconductor – in our case germanium or silicon.

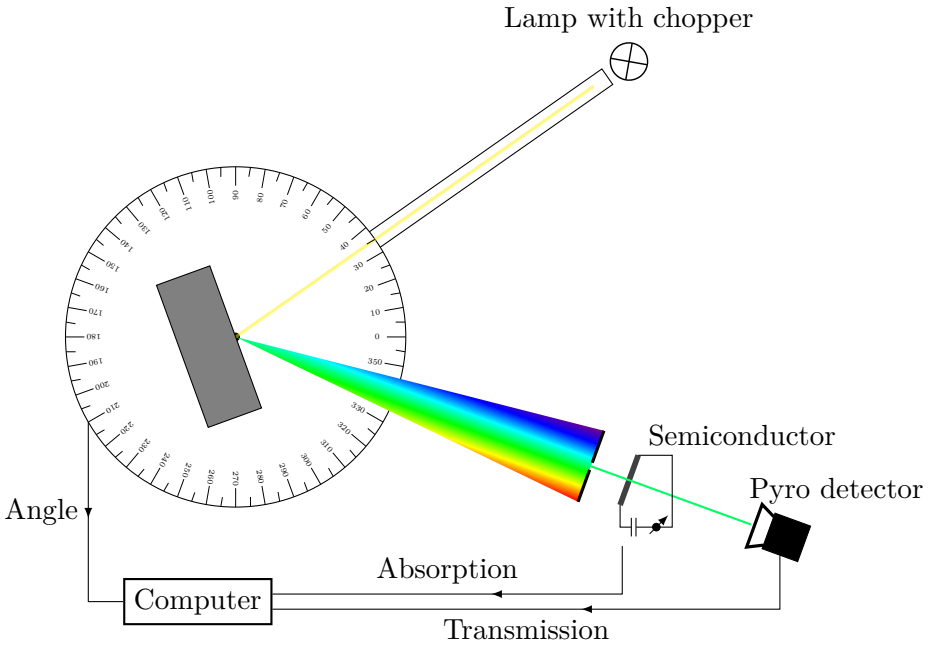


Figure 1: Setup for the determination of the band gap energy.

By applying a voltage to the semiconductor continuously throughout the experiment and measuring the current passing through the sample, the resistance of the semiconductor can be measured. If a photon with an energy higher than the band gap energy reaches the semiconductor and hits a valence electron, the latter can switch to the conducting band and contribute to the overall conductivity. As the grating differentiates the photons by their wavelengths and therefore by their energies, there exists an angle where all photons hitting the semiconductor have

exactly the band gap energy. This point can be measured by a sudden increase in conductivity. A so called pyro detector is mounted behind the semiconductor in order to quantify the transmission, i. e. the amount of photons passing through the semiconductor. The signal from the absorption as well as the signal from the transmission gets sent to a computer where it gets measured alongside the angle at which the grating is rotated. In order to filter out the noise, the transmission signal from the pyro detector gets sent to a lock-in amplifier before being transmitted to the computer. Because of the way the chopper pulses the light, the amplifier is able to filter out background signals not pulsed at 70 Hz by integrating over the signal.

### 2.1.2 Procedure

After switching on the lamp and the signal amplification as well as the motor control unit, the optical path is adjusted. Because the identification of an angle with a specific energy relies on the diffraction condition and therefore the use of parallel light, the position of the light used has to be adjusted, so that the light is mostly parallel when hitting the grating. Additionally, we configured the aperture to be about 1 cm wide. This was checked by holding a piece of paper in the path of the light at various positions on the optical bench and verifying the size of the beam. Next, the angle plate was rotated to zero (corresponding to the 0th maximum being diffracted right at the pyro detector) and the angle in the measurement program reset.

Our original plan was to start the measurement at the negative end of the angle range (about $-50°$ for the germanium sample) and measuring absorption and transmission using the slower setting of the motor of the angle plate until the positive end of the angle range was reached. However, while taking the measurement we noticed that the angle reported by the computer was about $10°$ off, which is why we proceeded to start at the zero angle and going to one end of the spectrum where we stopped the measurement, went back to zero and measured to the other end. Of course, this way of measuring the angle comes with huge potential for a systematic error as one has to reset the zero angle in between measurements. After taking a few series of measurement we noticed that the angle offset wasn't caused by the turn in direction of rotation, but rather the faster motor setting we used to reach one end of the spectrum. Because of the error potential, we discarded our prior measurements and proceeded by taking measurements starting at the zero angle, going to one end of the spectrum, switching direction, going to the other end of the spectrum and returning to the zero position, only using the slow motor setting. This allowed us to immediately see any offset by comparing the angle at the beginning of each measurement with the angle at the end.

Our first measurements with the method described above were carried out on a silicon sample. After taking the measurement, we removed the sample from the setup and repeated the measurement in order to quantify the power of the lamp with respect to the angle. Because without the sample the transmission data is amplified, we had to adjust the AC gain on the detector so that the signal wasn't driven into saturation. As we changed the amplification of the detector, the first measurement had to be repeated. After that, we went to the critical angle where we suspected the angle corresponding to the band gap energy to be and took mea-

surements of absorption and transmission without changing the angle in order to be able to quantify the scattering and therefore the error of the data. At last, we covered the semiconductor sample by closing the aperture and repeated the main measurement just like described above.

The next measurements were carried out on the germanium sample. After switching off the lamp and the power supply, we changed the sample, the grating and the filter, as described in the manual. The measurements were performed mostly in the same way, except that we started with the measurement without the sample, so that no amplification settings had to be changed during the experiment.

## 2.2 Analysis

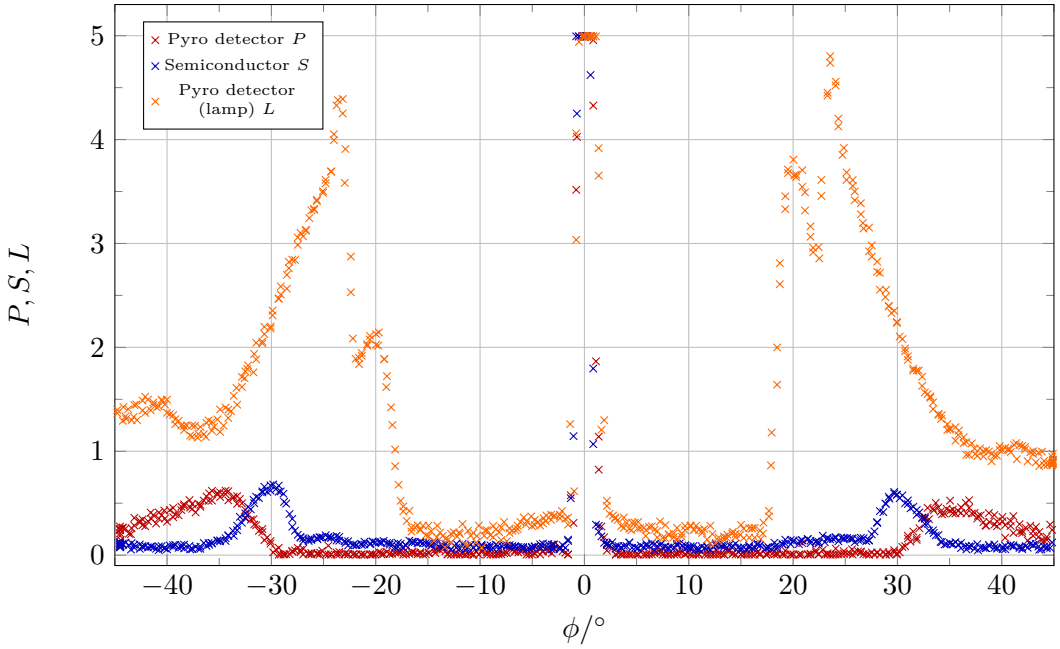


Figure 2: Main measurement and lamp measurement of the germanium semiconductor sample.

In this section, the measurements from the first part of the experiment analyzed. A discussion of the quality of the errors and the fits can be found in section 2.3. Since the data evaluation does not differ for the positive and negative angle range and both semiconductors, the evaluation of the positive angle range for germanium is carried out here as an example.

Underlying the analysis is the measurement series of the pyro detector and the semiconductor as well as the series of the pyro detector just with the lamp and the background series where the pyro detector and semiconductor measured while the aperture was closed. The main measurement is shown alongside the lamp measurement in fig. 2; the background measurement can be seen in fig. 19.

The manual suggested two methods of evaluation of which we chose the second. In order to be able to calculate an error and propagate it correctly, the error mea-

surement has to be the first to be analyzed: Let $P_i^{\mathrm{e}}, S_i^{\mathrm{e}}$ be the $i$-th measurement taken by the pyro detector and the semiconductor, respectively, during the error measurement. Furthermore, let $P$ be one data point from the pyro detector, $S$ a signal from the semiconductor (both taken during the main measurement) and $L$ the pyro signal during the lamp power measurement for a specific angle $\phi$. A good measure of uncertainty of these quantities is provided by the empiric standard deviation of their respective quantities during the error measurements:

$$\begin{aligned} s_P = s_L &= \frac{1}{N-1}\sqrt{\sum_{i=1}^{N}(P_i^{\mathrm{e}} - \overline{P^{\mathrm{e}}})^2} = 5.11 \times 10^{-2}\,\mathrm{V}, \\ s_S &= \frac{1}{N-1}\sqrt{\sum_{i=1}^{N}(S_i^{\mathrm{e}} - \overline{S^{\mathrm{e}}})^2} = 1.79 \times 10^{-2}\,\mathrm{V}, \end{aligned} \tag{5}$$

where $N$ is the number of data points measured during the error measurement. While one could argue that the variance of the quantities change for various angles, the fact remains that we are only interested in the course of absorption and transmission about the critical angle where the light has about the band gap energy. As such, the standard deviation should provide a good measure of error within a close region near the critical angle.

Before the data from the pyro detector and the semiconductor can be evaluated directly, the power of the lamp as well as the background has to be accounted for, first. As we examine the background measurements (cf. fig. 19), we notice that the distribution is mostly uniform noise and should be averaged out. However, because the second method of evaluation isn't affected by a shift of all values from the same measurement (as it only relies on intersections of lines from within one data set), subtracting an averaged background only adds to the error of the data. Therefore, we decided not to use our background measurement and proceeded with the further evaluation.

As already mentioned, the power of the lamp is not uniform at all (cf. fig. 18). In order to get a good measure for the transmission and the absorption, the pyro detector and semiconductor measurements have to be divided by the power of the lamp for each angle $\phi$. This is where we encountered a major problem in the way our data was taken: The computer only records the voltages reported by the pyro and semiconductor controllers at time intervals of 0.5 s alongside the angle $\phi$ at that time. Because the main measurement and the lamp measurement are separate series of measurement, their angles don't match up, which is why we can't simply compare their entries with each other. One possible solution to this is to bin the data with respect to the angle; however, this comes with the inconvenience to choose bin sizes and quantify the loss created by binning. Furthermore, our data set isn't nearly as large to support bin sizes so that the error on the angle can still be neglected. The other solution we came up with and ended up using was to extrapolate the data by extending both value lists: First, we created a list containing all possible values for the angle $\phi$. Then, we checked for each angle whether a data point (pyro or lamp pyro and sample or lamp pyro, respectively) exists. If it does, we add it to our extended list; if it doesn't, we search the measured data for the closest value and add that to the list. This method of extrapolation comes with the disadvantage that it shouldn't be used with many different series of measurement as it can create

a “staircase” effect in the data when too many data points are extrapolated. As we only have two series of measurement each that get processed in this way, we decided to use it nonetheless, as we thought it to be more reliable than the binning method.

After having cleaned our data in this way, we proceeded to define a measure for transmission and absorption which we will refer to with $\mathfrak{t}$ and $\mathfrak{a}$, respectively: Let $P, S, L$ be the data created and/or measured from the pyro detector, semiconductor and pyro detector within the lamp measurement, respectively, for one specific $\phi$. We can now define:

$$\mathfrak{t} = \frac{P}{L}, \qquad \mathfrak{a} = \frac{S}{L}. \tag{6}$$

The error on these quantities can be calculated using Gaussian error propagation:

$$\begin{aligned} s_\mathfrak{t} &= \sqrt{\left(\frac{s_P}{L}\right)^2 + \left(\frac{P}{L^2} \cdot s_L\right)^2}, \\ s_\mathfrak{a} &= \sqrt{\left(\frac{s_S}{L}\right)^2 + \left(\frac{S}{L^2} \cdot s_L\right)^2}. \end{aligned} \tag{7}$$

Now, we are able to plot the transmission and absorption graphically in the region where we suspected the angle belonging to the band gap energy to be. The plot is shown in fig. 3.

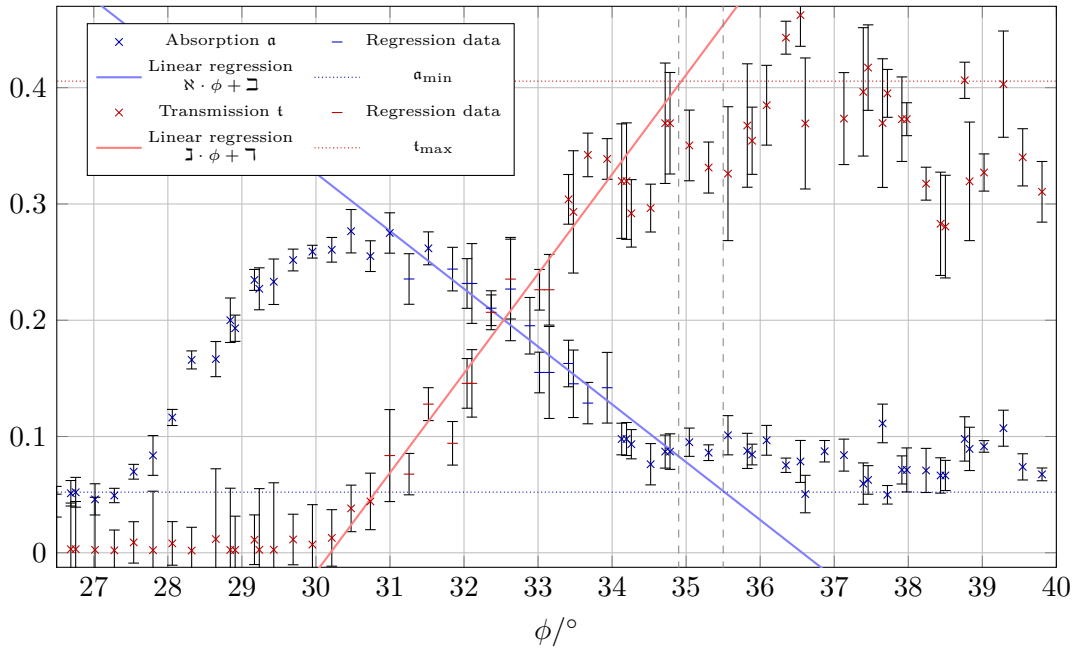


Figure 3: Plot of the absorption $\mathfrak{a}$ and transmission $\mathfrak{t}$ of the positive angle range of the germanium sample. Also shown is a linear regression with values given in eq. (9) as well as the intersection angles. The $\chi^2$ values are given in table 14.

Next, the maximum of the transmission curve $\mathfrak{t}_{\max}$ as well as the minimum of the absorption curve $\mathfrak{a}_{\min}$ are to be calculated. As our data set may very well contain statistical outliers, the weighted mean of the five largest/smallest values is taken in order to calculate $\mathfrak{t}_{\max}$ and $\mathfrak{a}_{\min}$. The extrema are shown by dashed lines in

the figure. Next, using the python module `scipy.optimize.curve_fit`, two linear regressions of the form

$$\begin{aligned} \mathfrak{t} &= \aleph \cdot \phi + \beth, \\ \mathfrak{a} &= \gimel \cdot \phi + \daleth \end{aligned} \tag{8}$$

were carried out for the transmission and absorption values, respectively, where $\aleph, \beth, \gimel$ and $\daleth$ are parameters of regression. We selected the data used for the regression so that it deviated approximately one standard deviation from the data points that we were sure would not contribute to the linear relationship[1]. The data used for the regression is marked by a minus ("−") marker in fig. 3. The results from the regression are

$$\begin{aligned} \aleph &= (8.558 \pm 0.009) \times 10^{-2}\, \frac{1}{\circ}, \\ \beth &= -2.58 \pm 0.09, \\ \gimel &= (-4.970 \pm 0.003) \times 10^{-2}\, \frac{1}{\circ} \\ \text{and } \daleth &= 1.82 \pm 0.03. \end{aligned} \tag{9}$$

The errors were calculated using the covariance matrix provided by the python module.

The intersection between the regression curves and the maximum transmission/minimum absorption lines is given by

$$\begin{aligned} \phi_{\mathfrak{t}} &= \frac{\mathfrak{t}_{\max} - \beth}{\aleph} = (34.9 \pm 2.7)^\circ \\ \text{and } \phi_{\mathfrak{a}} &= \frac{\mathfrak{a}_{\min} - \daleth}{\gimel} = (35.5 \pm 2.8)^\circ. \end{aligned} \tag{10}$$

The error on these values was calculated by inserting the variance $s^2_{\mathfrak{t}_{\max}}$ of $\mathfrak{t}_{\max}$ in the covariance matrix given by the python module and using Gaussian error propagation:

$$s^2_{\phi_{\mathfrak{t}}} = \begin{pmatrix} \frac{\partial \phi_{\mathfrak{t}}}{\partial \aleph} & \frac{\partial \phi_{\mathfrak{t}}}{\partial \beth} & \frac{\partial \phi_{\mathfrak{t}}}{\partial \mathfrak{t}_{\max}} \end{pmatrix} \cdot \begin{pmatrix} s^2_{\aleph} & \operatorname{cov}(\aleph, \beth) & 0 \\ \operatorname{cov}(\beth, \aleph) & s^2_{\beth} & 0 \\ 0 & 0 & s^2_{\mathfrak{t}_{\max}} \end{pmatrix} \cdot \begin{pmatrix} \frac{\partial \phi_{\mathfrak{t}}}{\partial \aleph} \\ \frac{\partial \phi_{\mathfrak{t}}}{\partial \beth} \\ \frac{\partial \phi_{\mathfrak{t}}}{\partial \mathfrak{t}_{\max}} \end{pmatrix} \tag{11}$$

Taking the weighted mean of both angles given in eq. (10) and propagating the error in the usual way yields

$$\phi_{\mathrm{g}} := \frac{\frac{\phi_{\mathfrak{t}}}{s^2_{\phi_{\mathfrak{t}}}} + \frac{\phi_{\mathfrak{a}}}{s^2_{\phi_{\mathfrak{a}}}}}{\frac{1}{s^2_{\phi_{\mathfrak{t}}}} + \frac{1}{s^2_{\phi_{\mathfrak{a}}}}} = (35.2 \pm 1.9)^\circ. \tag{12}$$

The band gap energy of germanium matches the energy corresponding to the angle $\phi_{\mathrm{g}}$ which can be calculated to be [3]

$$E_{\mathrm{g}} = \frac{hc}{2d \sin \phi_{\mathrm{g}} \cos \psi} = (6.5 \pm 0.3) \times 10^{-1}\,\mathrm{eV}, \tag{13}$$

[1] E. g. the transmission values with $\phi < 30^\circ$ in fig. 3.

of which the systematic error was computed using Gaussian error propagation:

$$s_{E_\mathrm{g}}^{\mathrm{stat}} = \frac{hc\cos\phi_\mathrm{g}}{2d\sin^2\phi_\mathrm{g}} \cdot s_{\phi_\mathrm{g}}. \tag{14}$$

However, the measurement of the band gap energy is also affected by a systematic error. Because of inadequacies in the experiment's setup (based on non-infinitesimal aperture width and grating), the energies hitting the sample aren't defined sharply and stem rather from an energy interval. This interval is bound by low-energy photons hitting the sample at an angle of $\phi_\mathrm{min}$ on the one end and high-energy photons arriving at an angle of $\phi_\mathrm{max}$ on the other end [2, p. 41]. By geometric means one arrives at

$$\begin{aligned} \phi_\mathrm{min} &= \psi + \arcsin\left(\frac{L\sin\psi - D/2\cos\phi_\mathrm{g} - B/2\cos\psi}{L}\right), \\ \text{and } \phi_\mathrm{max} &= \psi + \arcsin\left(\frac{L\sin\psi + D/2\cos\phi_\mathrm{g} + B/2\cos\psi}{L}\right), \end{aligned} \tag{15}$$

where $D = 2.5\,\mathrm{cm}$ denotes the width of the optical grating, $L$ is the distance between grating and lens which we measured to be $45.5\,\mathrm{cm}$ and $B = 1.2\,\mathrm{cm}$ is the aperture width. Using these angles, one can calculate the systematic error caused by the setup:

$$s_{E_\mathrm{g}}^{\mathrm{sys}} = \frac{hc}{4B\cos\psi}\left(\frac{1}{\sin\left(\phi_\mathrm{min}/2\right)} + \frac{1}{\sin\left(\phi_\mathrm{max}/2\right)}\right) = 4.77\times10^{-5}\,\mathrm{eV} \tag{16}$$

Comparing the statistical error with the systematic error calculated just now, we notice that the latter can be neglected. Equation (13) thus contains the final result for the band gap energy of germanium using the positive angle range.

Continuing the evalutation in exactly the same way as described above yields the band gap energy of germanium from the negative angle range. The energy is shown alongside important fit parameters in tables 13 and 15. The latter also contains the systematic error as calculated in eq. (16).

Taking the weighted average of the band gap energies of both angle ranges yields the following band gap energies:

$$\begin{aligned} \text{Germanium: } E_\mathrm{g} &= (6.4 \pm 0.2)\times10^{-1}\,\mathrm{eV}, \\ \text{Silicon: } E_\mathrm{g} &= (1.08 \pm 0.02)\,\mathrm{eV}. \end{aligned} \tag{17}$$

Table 14 contains the relevant $\chi^2$- and reduced $\chi^2_\nu$-values for both fits of each angle range for both semiconductors.

## 2.3 Discussion

In the first part of the experiment, the band gap energies of germanium and silicon were determined to the following values:

$$\begin{aligned} \text{Germanium: } E_\mathrm{g} &= (6.4 \pm 0.2)\times10^{-1}\,\mathrm{eV}, \\ \text{Silicon: } E_\mathrm{g} &= (1.08 \pm 0.02)\,\mathrm{eV}. \end{aligned}$$

Comparing these values to their literature values of $6.6 \times 10^{-1}\,\mathrm{eV}$ and $1.12\,\mathrm{eV}$ for germanium and silicon [3], respectively, we note that the value for germanium lies within a $1\sigma$-environment of the literature value, while our result for silicon lies just within a $2\sigma$-envorinment from its literature value. Thus, our findings confirm the literature values within the scope of accuracy of our experiment.

However, the technical correctness of our results shouldn't refract from the fact that our band gap energies come with an error that seems misleadingly small: Looking exemplarily at the band gap energy of the positive angle range of germanium given by eq. (13), we can see that the error (which is on the same order of magnitude as our error on the final result) stems from the error on the angle $\phi_\mathrm{g}$ which is given in eq. (12). If we now compare the error on this angle ($1.9°$) with scale in fig. 3, we see that the error on the angle is quite large when compared with the dashed vertical lines which form the boundaries of the band gap energy angle $\phi_\mathrm{g}$.

When tracing back the error it seems as the main source of the high uncertainty was due to the high error on the fit parameters (given by eq. (9)) used for the linear regressions. It stands to reason that the cause for the doubtfulness of the fit seems to lie in the scarcity and quality of data actually used in the regression: As one can see in fig. 3, the amount of data contributing to the linear relationship is rather marginal when compared with the rest of the data set.

Furthermore, it should be noted that next to the scarcity of the regression data the quality of this data must also be taken into account: In order to be able to use data from two different series of measurement, we had to extrapolate some data which could exacerbate the quality of the fit considerably, if the fit region contains a lot of extrapolated data.

Both of the above mentioned error sources can be solved by a modification of the experiment's setup: If one were to use a digital motor control which can be set to specific angles by a computer program for example, one would eliminate the need for data extrapolation. Additionally, by using a finer resolution, the matter of the rather marginal data amounts in the critical region can also be dealt with. This can also be accomplished by using a motor which can be set to be just slower in general.

Another thing to add is that each of the band gap energies appear to be lower than the literature value. This may be due to some systematic error in the way our angles were measured: If, for example, the scale of the angle measurement was slightly off with regard to the voltage controller measurements, the angle measurements won't correspond exactly with the pyro detector and sample data points.

All in all we can conclude that in spite of having arrived at an acceptable result for the band gap energies, the error on this result is actually quite disproportionate and presumably due to low source data density in critical fit regions.

# 3 Haynes and Shockley experiment

This part is a modified version of the Haynes and Shockely experiment. By observing the movement of a charge carrier cloud caused by a laser, the mobility $\mu$, the mean life time $\tau$ and the diffusion constant $D$ of a p doped germanium sample will be determined.

## 3.1 Setup and procedure

### 3.1.1 Setup

For this experiment a p-doped germanium semiconductor is used at which a voltage can be applied. In order to reduce the heating the voltage is applied in pulses: If the voltage was applied all the time, the germanium sample could warm up and thus change its conductive properties. Laser pulses can be directed at the germanium sample with an optical fiber cable to generate free charge carriers in the germanium sample. Because the field applied needs a short time to get into balance, the laser pulses a short time after the voltage is switched on In order to measure the free charge carriers, a needle is connected to the germanium sample. The signal from the needle can be observed on an oscilloscope. In order to observe the relatively weak signal of the carrier cloud, the needle signal is modified by an additional voltage to subtract the offset by the electric field. A second channel of the oscilloscope can be used to observe the voltage applied to the germanium. The oscilloscope can be triggered externally at the beginning of the laser pulse. Optical fiber cable and needle are mounted in such a way that their distance from each other can be varied.

### 3.1.2 Procedure

For the entire experiment, we had set the maximum amplitude of the laser to obtain the largest possible signals. During measurements for different distances, the voltage was set to $(50 \pm 2)\,\mathrm{V}$. In order to set the voltage, we had to adjust the time scale to a range of $250\,\mu\mathrm{s}$. When adjusting the distance, we switched off the voltage and the laser to prevent damage to the equipment from short circuits. We used a caliper to adjust the distance between needle and laser by setting the caliper to the wanted distance, putting it next to our setup and then moving the optical fiber cable until it reached the caliper. After we adjusted the distance, the laser and voltage was turned on again. While the time resolution was set to $100\,\mu\mathrm{s}$ we adjusted the 'Level Shift' to annihilate the voltage applied to the germanium sample. We reduced the time resolution until we could see the Gaussian as well as possible. While reducing the time resolution, we normally had to readjust the level shift.

The procedure was the same for all different distances: First, we did a series of measurements from 2.01 mm to 9.01 mm in steps of ca. 1 mm. After completing this series, we decided to do a second series of measurements in which we used the stop function of the oscilloscope in order to improve the signals.

For the second measurements we started at 1.51 mm going to 7.00 mm. Up to ca. 4 mm we used steps of about 0.5 mm and from then on again steps of ca. 1 mm. For the measurements with one fixed distance and different voltages we adjusted the distance to $(4.01 \pm 0.01)\,\mathrm{mm}$. To adjust the voltage we set the time scale to

250 µs like before. Afterwards, we redid the adjustment of the 'Level Shift' and the reducing of the scale same as with the other measurements. We measured for voltages from ca. 50 V to 15 V in steps of 5 V.

## 3.2 Analysis

### 3.2.1 Variation of the distance

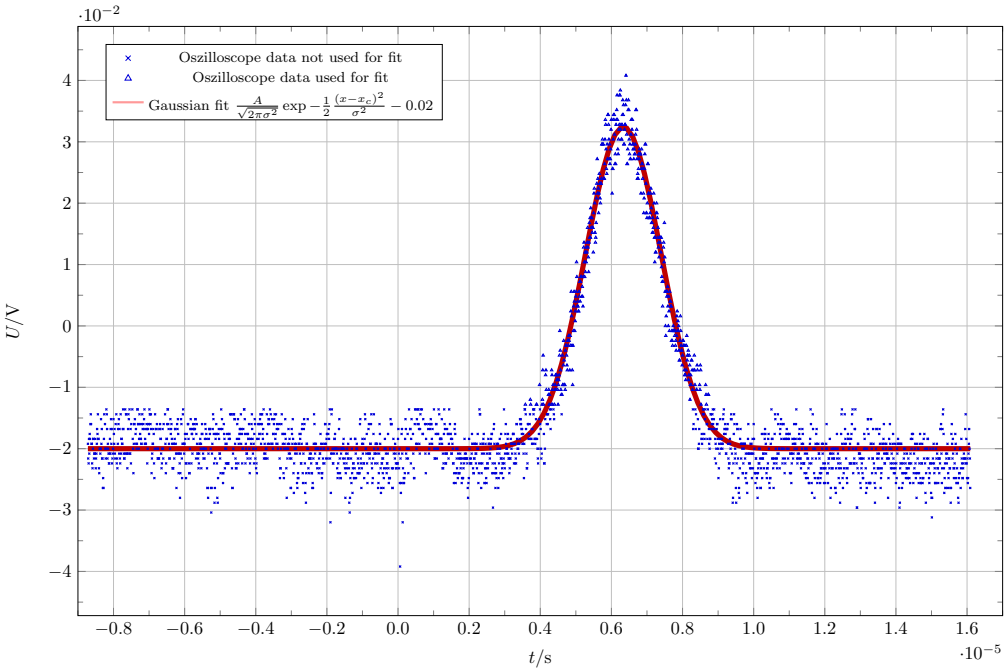


Figure 4: Measurement with the distance $d = 1.99\,\mathrm{mm}$ with $\chi^2_\nu = 2.86$.

To obtain the mean life time $\tau$, mobility $\mu$ and diffusion constant $D$ the data taken from the oscilloscope for each distance was fitted with a Gaussian:

$$f(x) = \frac{A}{2\pi\sigma^2} e^{-\frac{1}{2}\frac{(x-x_c)^2}{\sigma^2}} + c \tag{18}$$

Here, $A$, $\sigma$ and $x_c$ are the parameters of the fit, while $c$ is obtained by the mean of the data not used for the fit.

We selected the data for the fits by setting a maximum voltage we thought the background data would not exceed and taking the data points above this boundary. This is shown exemplary in fig. 4, where we set the boundary voltage at about $-1.2\,\mathrm{V}$. The fits were carried out by using the non-linear least squares python fitting module `scipy.optimize.curve_fit`. Table 16 shows the values of the fit parameters for the second measurement series. The errors of the fit parameters were calculated using the covariance matrix provided by the python module. In addition, the reduced chi-squared $\chi^2_\nu$ were calculated and are noted in the caption of each plot. For example, the fit to the measurement with the distance $d = 1.51\,\mathrm{mm}$ is shown in fig. 4; the other plots can be found in the appendix.

| $d$/mm | $A$/V s | $\sigma$/s | $xc$/s |
|---|---|---|---|
| 1.51 | $1.384 \pm 0.008 \times 10^{-7}$ | $1.057 \pm 0.008 \times 10^{-6}$ | $6.335 \pm 0.007 \times 10^{-6}$ |
| 1.99 | $2.423 \pm 0.013 \times 10^{-7}$ | $1.200 \pm 0.007 \times 10^{-6}$ | $8.300 \pm 0.007 \times 10^{-6}$ |
| 2.50 | $2.996 \pm 0.130 \times 10^{-7}$ | $1.243 \pm 0.007 \times 10^{-6}$ | $8.392 \pm 0.006 \times 10^{-6}$ |
| 3.00 | $8.31 \pm 0.12 \times 10^{-8}$ | $1.64 \pm 0.03 \times 10^{-6}$ | $1.008 \pm 0.002 \times 10^{-5}$ |
| 3.49 | $7.17 \pm 0.19 \times 10^{-8}$ | $1.68 \pm 0.06 \times 10^{-6}$ | $1.132 \pm 0.004 \times 10^{-5}$ |
| 4.01 | $6.45 \pm 0.13 \times 10^{-8}$ | $1.81 \pm 0.05 \times 10^{-6}$ | $1.272 \pm 0.004 \times 10^{-5}$ |
| 5.00 | $7.78 \pm 0.08 \times 10^{-8}$ | $1.021 \pm 0.014 \times 10^{-6}$ | $1.0889 \pm 0.0012 \times 10^{-5}$ |
| 6.00 | $5.72 \pm 0.11 \times 10^{-8}$ | $1.11 \pm 0.03 \times 10^{-6}$ | $1.312 \pm 0.002 \times 10^{-5}$ |
| 7.00 | $6.22 \pm 0.17 \times 10^{-8}$ | $1.47 \pm 0.05 \times 10^{-6}$ | $1.486 \pm 0.003 \times 10^{-5}$ |

Table 3: Fit parameters for the Gaussian fits of the second series of measurement by varying the distance.

The Gaussian curves obtained in this way for the second series of measurements are plotted together in fig. 5. As can be seen in this plot, the Gaussian curves deviate from the expected pattern.

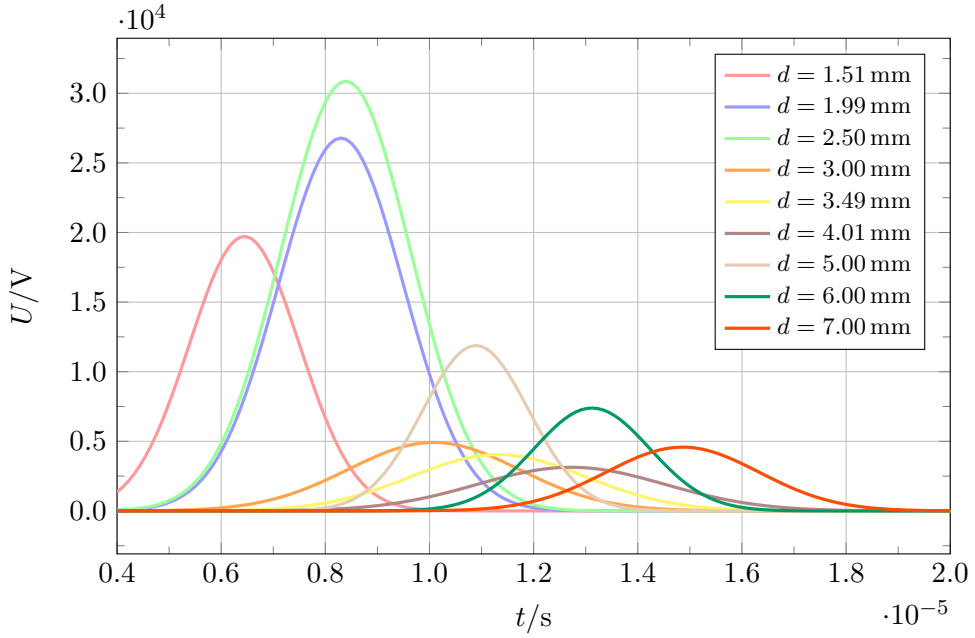


Figure 5: The Gaussian fits for different distances of the second series of measurements.

Therefore, we decided to evaluate the first series of measurements we originally decided to discard. However, only the first four measurements were used, as the remaining ones do not have a strong enough signal to properly fit a Gaussian. The values for the fit parameters of this series of measurements can be seen in table 16. As for the others, the Gaussian curves are plotted together in fig. 6. The Gaussian curves of this measurement series correspond more closely to the expected pattern.

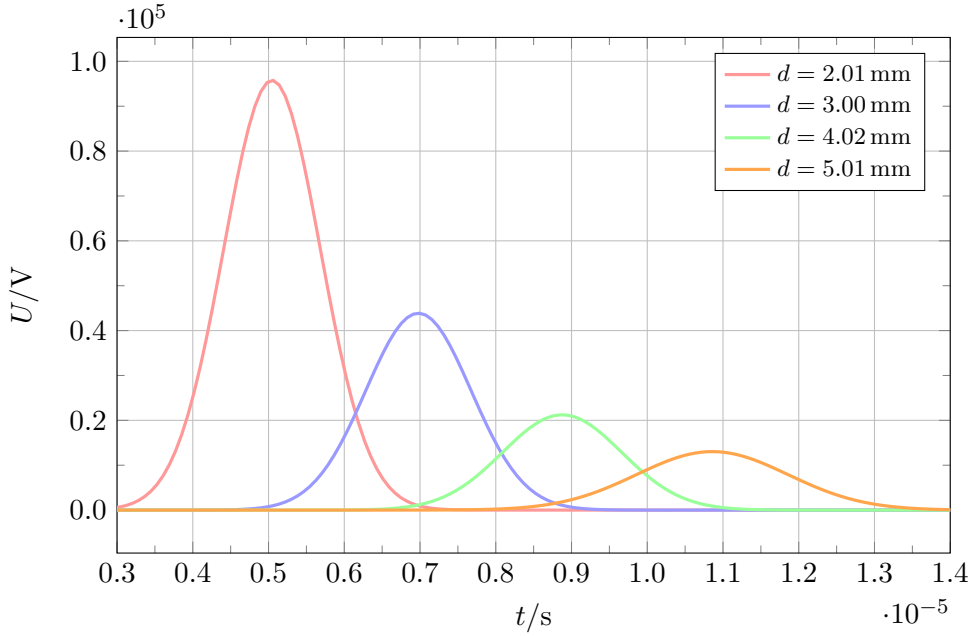


Figure 6: The Gaussian fits for different distances of the first series of measurements.

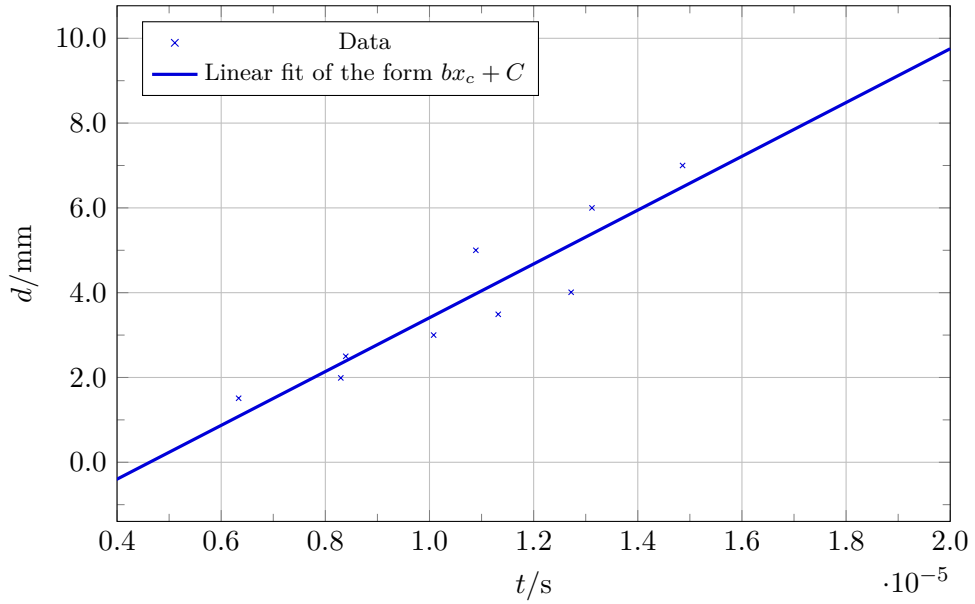


Figure 7: Linear fit of the form $d = b \cdot x_c + C$ to determine $\mu$. Second series of measurements.

| Series of measurement | $b/\frac{\text{mm}}{\text{s}}$ | $C$/mm | $\chi^2_\nu$ |
|---|---|---|---|
| 1 | $5.18 \pm 0.05 \times 10^5$ | $-0.60 \pm 0.04$ | 0.05 |
| 2 | $6.0 \pm 1.0 \times 10^5$ | $-2.9 \pm 1.1$ | 58 |

Table 4: Fit parameter of the linear regression to determine the mobility of the measurements with varying the distance.

If one compares eqs. (4) and (18), one can see that there is the following correlation between the mobility $\mu$, the measured distances and the fit parameter $x_c$:

$$d = \mu E t \tag{19}$$

Thus, $\mu$ can be determined by plotting the measured distances over the respective mean values of the Gaussian curves and the carrying out a linear regression. This was done again by using the python module `scipy.optimize.curve_fit`, separately for both measurement series. The obtained values for the fit parameters are shown in table 4. The corresponding plots are shown in fig. 7 for the second measurement series and in fig. 24 for the first.

To calculate $\mu$, the slope obtained must be divided by the energy of the electric field $E$, which can be described by $E = \frac{U}{l}$. $U$ is the voltage applied to the semiconductor and was measured as $U = (50 \pm 1)\,\mathrm{V}$ and $l = 30\,\mathrm{mm}$ is the length of the germanium sample. In this way $\mu$ was calculated with the first series of measurements to

$$\mu_1 = (3110 \pm 130)\,\frac{\mathrm{cm}^2\,\mathrm{s}}{\mathrm{V}} \tag{20}$$

and with the second series of measurements to

$$\mu_2 = (3800 \pm 600)\,\frac{\mathrm{cm}^2\,\mathrm{s}}{\mathrm{V}}. \tag{21}$$

The error was calculated the same in both cases by using Gaussian error propagation:

$$s_\mu = \sqrt{\left(\frac{bl}{U^2} s_U\right)^2 + \left(\frac{l}{U} s_b\right)^2} \tag{22}$$

If one compares eqs. (4) and (18) again, the following relationship can also be stated:

$$A(t) = b e^{-\frac{t}{\tau}} \tag{23}$$

Therefore, the fit parameters $A$ were plotted over the fit parameters $x_c$ and fit exponentially. $\tau$ can then simply be determined as one of the fit parameters. For both series of measurements the fit parameters are listed in table 5. The plot of the first series of measurements can be seen in fig. 25 and for the second in fig. 8. With the fit of the first series of measurements $\tau$ was determined as

$$\tau_1 = (3.4 \pm 0.4) \times 10^{-6}\,\mathrm{s} \tag{24}$$

and with the one of the second as

$$\tau_2 = (8 \pm 5) \times 10^{-6}\,\mathrm{s}. \tag{25}$$

For the determination of the diffusion constant

$$\sigma_\mathrm{R}(t) = \sqrt{2Dt} \tag{26}$$

| Series of measurement | $b$/V s | $\tau$/s | $\chi^2_\nu$ |
|---|---|---|---|
| 1 | $1.1 \pm 0.4 \times 10^{-6}$ | $3.4 \pm 0.4 \times 10^{-6}$ | 350 |
| 2 | $4 \pm 3 \times 10^{-7}$ | $8 \pm 5 \times 10^{-6}$ | 3634 |

Table 5: Fit parameter of the exponential fit to determine the mean life time of the measurements with varying the distance.

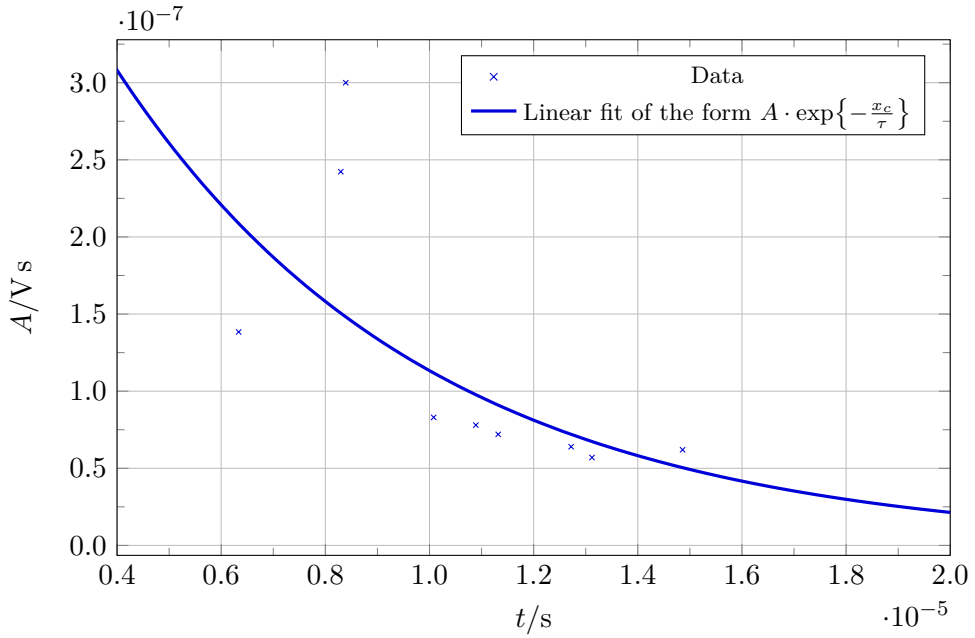


Figure 8: Exponential fit of the form $A = b \cdot e^{-\frac{x_c}{\tau}}$ to determine $\tau$. Second measurements.

| Series of measurement | $D$/V | $\chi^2_\nu$ |
|---|---|---|
| 1 | $1.0 \pm 0.5 \times 10^4$ | 22.8 |
| 2 | $2.7 \pm 4.0 \times 10^4$ | 1.6 |

Table 6: Fit parameter of the square root fit to determine the diffusion constant of the measurements with varying the distance.

can be used. This correlation follows from the comparison of eqs. (4) and (18). $\sigma_\mathrm{R}$ is the spatial standard deviation obtained by multiplying the temporal standard deviation $\sigma$ by the velocity of the electron cloud:

$$\sigma_\mathrm{R} = \sigma \cdot v = \mu \cdot E \tag{27}$$

Therefore, the $\sigma$ obtained by the Gaussian fits is multiplied with the fit parameter $b$ in table 4. The error of $\sigma_\mathrm{R}$ was calculated with the use of Gaussian error propagation. Then, $\sigma_\mathrm{R}$ was plotted over $x_c$ and a fit of the form eq. (26) was fitted; again using the python module `scipy.optimize.curve_fit`. The fit parameters are shown in table 6, while the plot for the first series of measurements is in fig. 26 and for the second in fig. 9. For the first series of measurements the diffusion constant obtained is

$$D_1 = (101 \pm 5)\,\frac{\mathrm{cm}^2}{\mathrm{s}} \tag{28}$$

and for the second

$$D_2 = (280 \pm 40)\,\frac{\mathrm{cm}^2}{\mathrm{s}}. \tag{29}$$

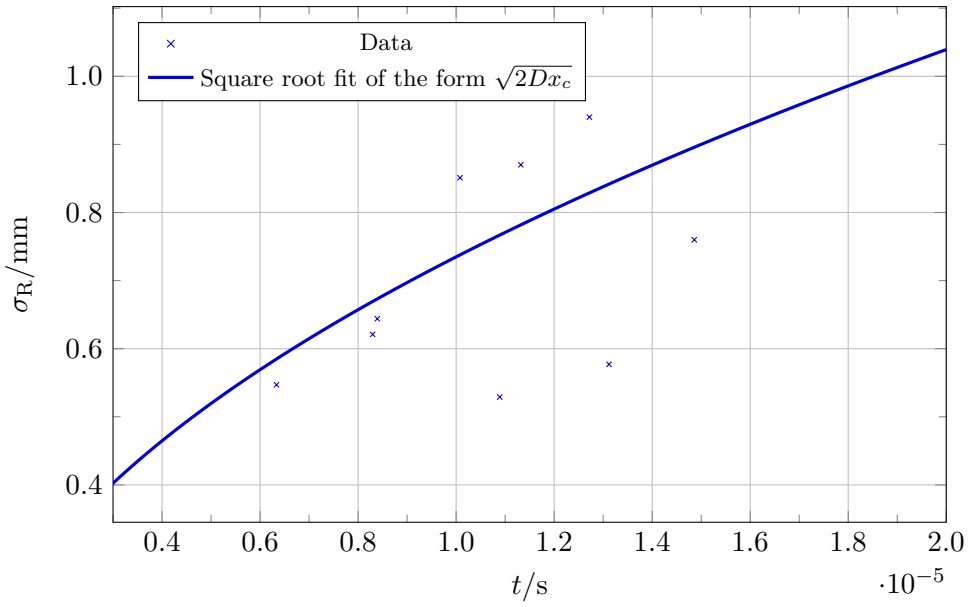


Figure 9: Square root fit of the form $\sigma_\mathrm{R} = \sqrt{2Dx_c}$ to determine $D$. Second series of measurements.

| $U$/V | $A$/V s | $\sigma$/s | $xc$/s |
|---|---|---|---|
| 49.6 | $9.96 \pm 0.08 \times 10^{-8}$ | $8.54 \pm 0.08 \times 10^{-7}$ | $9.852 \pm 0.007 \times 10^{-6}$ |
| 44.8 | $9.41 \pm 0.18 \times 10^{-8}$ | $1.37 \pm 0.03 \times 10^{-6}$ | $1.079 \pm 0.003 \times 10^{-5}$ |
| 40.0 | $6.14 \pm 0.15 \times 10^{-8}$ | $1.16 \pm 0.04 \times 10^{-6}$ | $1.199 \pm 0.002 \times 10^{-5}$ |
| 35.2 | $1.14 \pm 0.03 \times 10^{-7}$ | $1.83 \pm 0.06 \times 10^{-6}$ | $1.292 \pm 0.004 \times 10^{-5}$ |

Table 7: Fit parameters of the Gaussian fits of the measurements by varying the voltage applied to the semiconductor.

### 3.2.2 Variation of the voltage

For the variation of the voltage, also the data from the oscilloscope were fitted with eq. (18). Only the four measurements with the highes voltages were used, since the others do not provide a strong enough signal to make a Gaussian fit. The obtained fit parameters are shown in table 7. As for the distance measurements, the Gaussian were plotted together, which can be seen in fig. 10.

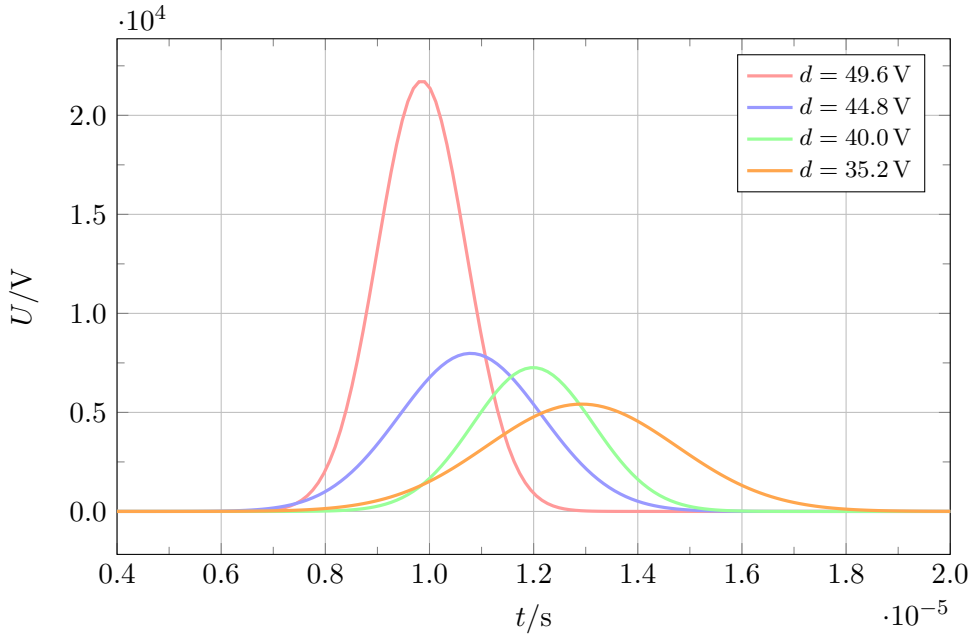


Figure 10: The gaussian fits for different voltages.

In order to determine $\mu$, eq. (19) is transposed to:

$$U = \frac{ld}{\mu t} \tag{30}$$

Therefore $U$ was plotted over $x_c$ and fitted with a fit of the form

$$U = \frac{b}{t} + C \tag{31}$$

using the python module `scipy.optimize.curve_fit`. The fit parameters were

determined as:

$$b = (5.8 \pm 0.4) \times 10^{-5} \,\frac{\mathrm{V}}{\mathrm{s}} \tag{32}$$

$$C = (-9 \pm 3)\,\mathrm{V} \tag{33}$$

and the reduced $\chi^2 = 0.7$. $\mu$ is calculated with

$$\mu = \frac{ld}{b} \tag{34}$$

were $l = 30\,\mathrm{mm}$ is the length of the germanium sample and $d = (4.01 \pm 0.05)\,\mathrm{mm}$ is the adjusted distance between needle and laser. This leads to

$$\mu_U = (2060 \pm 130)\,\frac{\mathrm{cm}^2}{\mathrm{V\,s}}. \tag{35}$$

The error again is obtained by Gaussian error propagation. The method to determine $\tau$ is the same as for the variation of the distance measurements. The obtained fit parameters are

$$b = (3 \pm 4)\,\mathrm{V\,s} \tag{36}$$

$$\tau_U = (8 \pm 7)\,\mathrm{s} \tag{37}$$

with which you directly get $\tau$. The reduced $\chi^2$ is calculated as $\chi^2_\nu = 166$ The fit and data is plotted in fig. 12. Also the diffusion constant was determined the same way as before. But here it must be noted that this time not every $\sigma$ was measured with the same voltage and therefore the respective voltage has to be used. The corresponding plot is shown in fig. 13. From the fit the diffusion constant

$$D_U = (4900 \pm 800)\,\frac{\mathrm{mm}^2}{\mathrm{s}} = (49 \pm 8)\,\frac{\mathrm{cm}^2}{\mathrm{s}} \tag{38}$$

was determined. Also the reduced $\chi^2$ was calculated to be $\chi^2_\nu = 48$.

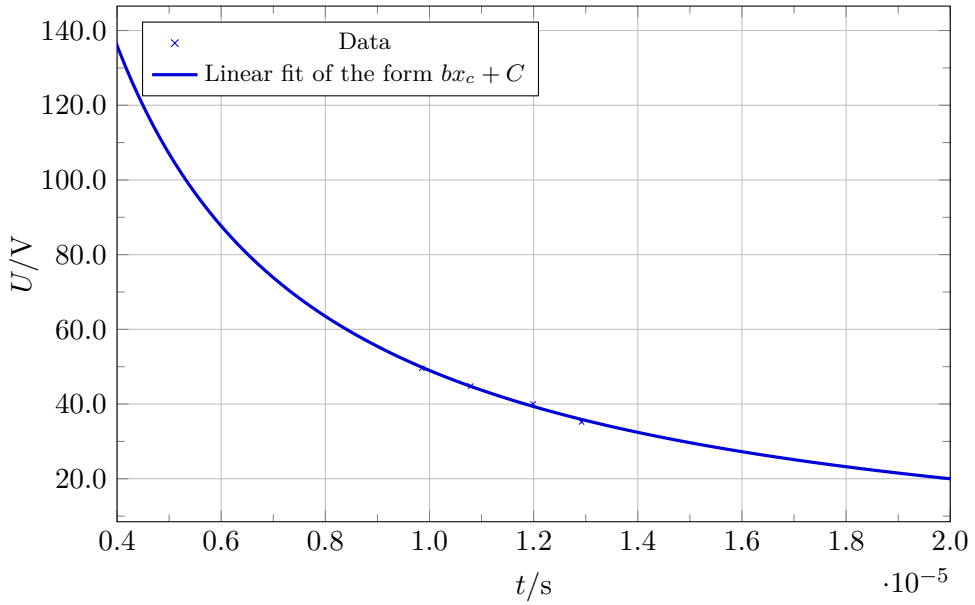


Figure 11: The fit of the measurements with varying voltages to determine the mobility $\mu$.

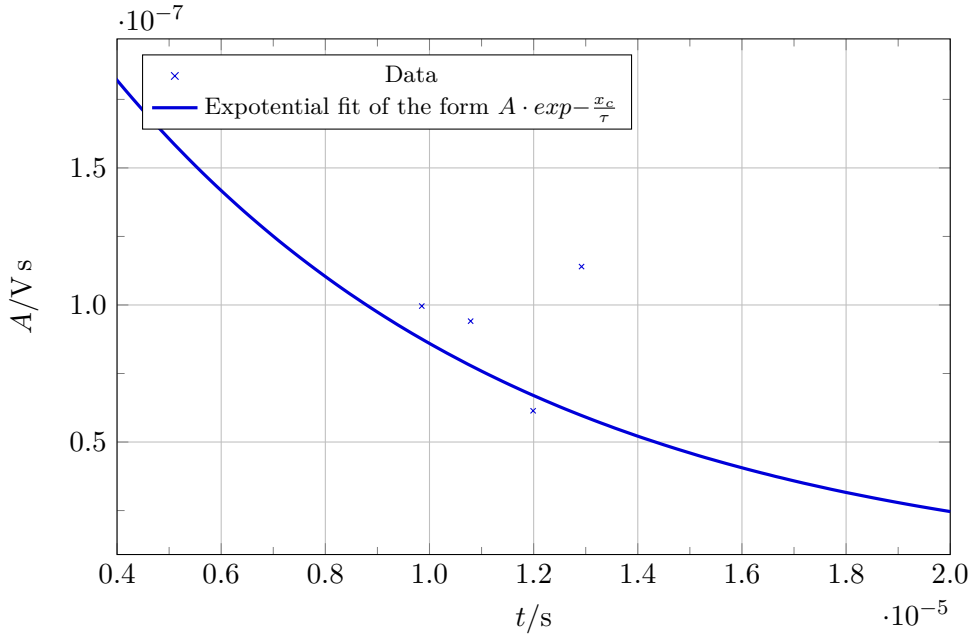


Figure 12: Exponential fit of the form $A = b \cdot e^{-\frac{x_c}{\tau}}$ to determine $\tau$.

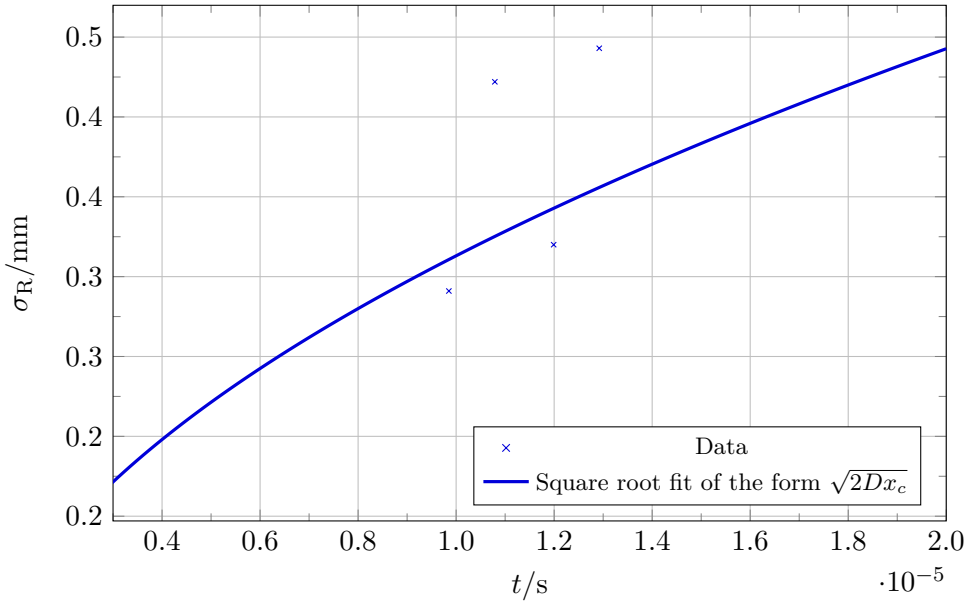


Figure 13: Square root fit of the form $\sigma_R = \sqrt{2Dx_c}$ to determine $D$.

| Method | $\mu / \frac{\text{cm}^2}{\text{Vs}}$ | $\tau$/s | $D / \frac{\text{cm}^2}{\text{s}}$ |
|---|---|---|---|
| Variation of distance 1 | $3110 \pm 130$ | $3.4 \pm 0.4$ | $101 \pm 5$ |
| Variation of distance 2 | $3800 \pm 600$ | $8 \pm 5$ | $280 \pm 40$ |
| Variation of voltage | $2060 \pm 130$ | $8 \pm 7$ | $49 \pm 8$ |
| literature values | 3900 | $45 \pm 2$ | 101 |

Table 8: Results of the different measurements for comparison.

### 3.3 Discussion

In order to compare the results of the different measurements, they were listed in table 8 together with the literature values. For the first series of measurements with varying the distance the literature value of the mobility $\mu$ lies in a $6\sigma$ environment, the literature value of the mean life time $\tau$ in a $104\sigma$ environment and the diffusion constant $D$ in a $1\sigma$ environment. For the second series of measurements the literature value of the mobility $\mu$ lies in a $1\sigma$ environment, the mean life time $\tau$ in a $8\sigma$ environment and the diffusion constant $D$ in a $5\sigma$ environment. At last for the measurements with varying the voltage, the literature value of the mobility $\mu$ lays in a $15\sigma$ environment, the mean time life $\tau$ in a $6\sigma$ environment and the diffusion constant $D$ in a $7\sigma$ environment.

First, the mean life time should be discussed. All values obtained are one order smaller than the literature value and lie within a similar value range among each other. This is probably due to the fact that crystal defects and other impurities in the semiconductor can greatly reduce the life time $\tau$. Since the laser only penetrates into the upper layers of the germanium sample, it can be reasoned that the sample used actually shows such defects which can also have an influence on $\mu$. Since the results of the distance measurements do not deviate as strongly from the literature

value as with the results for $\tau$, it can be assumed that the influence of the defects is not as strong as in $\tau$. For determining the diffusion constant $D$ the result of the first distance measurement is quite good, but that of the second deviates more. Also the result for $D$ from the measurements with different voltages diverges strongly from the literature value. Especially for the measurement with varying the voltage the small number of data which can be used reduces the precision of the results. Since four data point is not necessarily sufficient for fits and outliers have a greater influence. Therefore more different measurements with voltages in between 50 V and 35 V must have been taken.

For the measurements with varying the distance a series of measurements with more data was done; but as mentioned in section 3.2 when plotting the obtained Gaussian they differ strongly from the expected pattern. A direct reason for the second series of measurements differing much more from the expectation as the first series of measurements could not be determined. The only thing that was different in the measurements of the series of measurements is, that for the second one the stop function of the oscilloscope was used, but this should not influence the measurements like this. A peculiar thing to mention is that the Gaussian from the three biggest distances of the second series of measurements fit together quite well, as it can be seen in fig. 14. In addition to the mentioned defects of the sample, the glass fiber

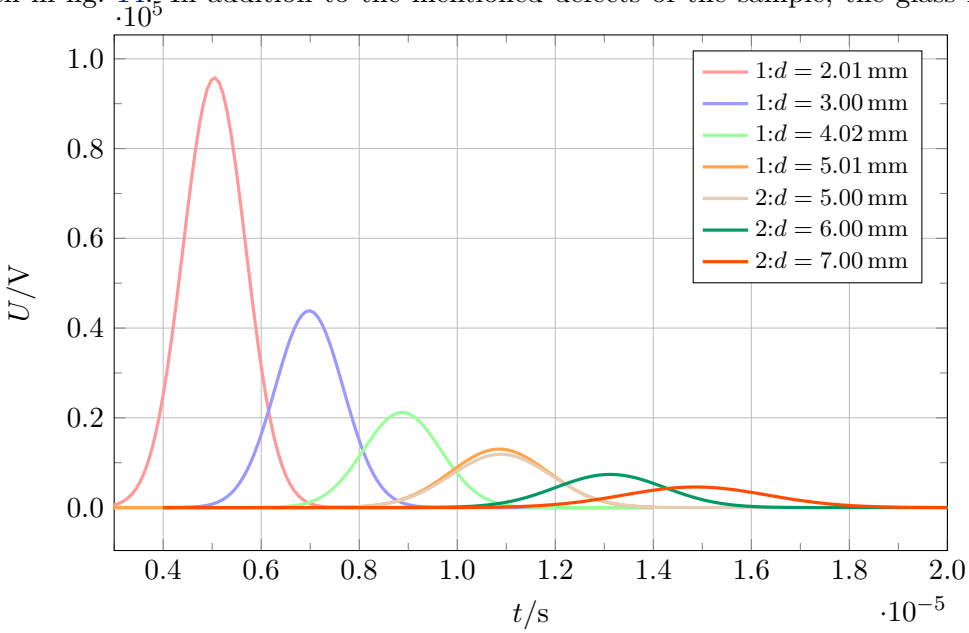


Figure 14: Plot to show that the Gaussian from the first series of measurements and the last three of the second series of measurements fit together quite well.

cable may be a source of error, too: As the glass fiber cable bends while it is being moved and touching the sample, repeated back-and-forth movement of the needle may have falsified the measurement of the distance. Also the bending changes the intensity with which the laser shoots at a point of the sample as the area hit by the beam changes when being hit at an angle. Furthermore, moving the glass fiber cable may results in shooting on parts of the sample with defects of varying severity, which would also falsify the measurements. All these aspects together could be the reason why the second measuring series by varying the distance deviates so strongly.

# 4 Semiconductor Detectors

The objective of the last part of the experiment was to examine the application of semiconductor detectors as particle detector and gain a rough insight into the their functionality.

In the experiment, two radioactive sources were used: $^{57}$Co which mainly decays in a $\beta$-decay with an energy of 59.5 keV and $^{241}$Am featuring two decays of interest with energies of 122.06 keV and 136.47 keV. The half-life time of the americum sample amounts to 432.7 a [1, 11–13,11-192].

## 4.1 Setup and Procedure

### 4.1.1 Setup

The experimental setup for this part of the experiment is relatively simple by way of comparison with the other parts: A semiconductor detector picks up a signal from a radioactive source and sends a current signal to the pre-amplifier where the signal gets converted into a voltage signal. After that, the signal passes through a shaping amplifier which smooths the sharp voltage edge by transforming it into a Gaussian-like voltage peak. This peak can be picked up by the multi-channel analyzer (MCA) which converts the analog peak into a digital signal by assigning a specific channel based on the amplitude of the voltage signal and therefore the corresponding photon energy. The counts of events sorted by the MCA channel can now be evaluated using a computer. The basic setup is sketched in fig. 15.

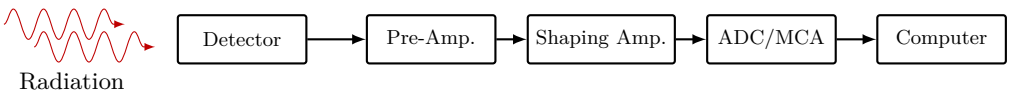


Figure 15: Schematic setup of the semiconductor detector part of the experiment

### 4.1.2 Procedure

After making sure the semiconductor detector is placed in the appropriate housing, the radioactive source was placed on top of the housing. Then, the connection to the computer was verified and the measurements started. The first measurements were carried out on the radioactive americum source using a silicon diode. After taking the measurement for one hour, we switched to the CdTe detector and measured the same source for another hour. We then proceeded to take background measurements (i. e. removing the source and starting a measurement) of both detectors, measuring half an hour each. Lastly, the cobalt source was examined. After taking one one-hour measurement for each detector, we decided to extend both of these measurements for another hour as the relevant peaks didn't show the desired intensities in the diagram shown by the computer.

## 4.2 Analysis

In the first part of the analysis, the parameters of the linear relationship between energy of the photons stemming from the radioactive source and the channels will be

determined from our measured data. Then, the absorption ratios of both semiconductor detectors will be determined for each of the energy peaks. Lastly, the relative energy resolution of each energy will be calculated for both of the semiconductor detectors.

### 4.2.1 Energy calibration

In order to find the parameters of the linear relationship between photon energy and MCA channel, one has to carry out a linear regression on a data set where the energies of known peaks are plotted against their MCA channel. As we know that the americum sample features a peak at 59.5 keV and the peaks of the cobalt sample lie at 122.06 keV and 122.06 keV, the remaining task is to find their respective channels for each of the semiconductors. Before that, the measured background has to be subtracted for each energy channel. Let $N_i$ be the bin content of the main measurement of the $i$th bin, $M_i$ the counts of the background measurement of the same bin. The "correct" count $n_i$ created by the radioactive source is given as

$$n_i = N_i - \frac{t_M}{t_N} M_i, \tag{39}$$

where $t_N, t_M$ are the total measurement times of the main or background measurement, respectively. The error on $n_i$ can be calculated by the use of Gaussian error propagation and the assumption that the channel contents are distributed according to a Poisson distribution:

$$s_{n_i} = \sqrt{s_{N_i}^2 + \frac{t_M^2}{t_N^2} s_{M_i}^2} = \sqrt{N_i + \frac{t_M^2}{t_N^2} M_i} \tag{40}$$

By fitting a modified Gaussian distribution

$$\frac{\aleph}{\sqrt{2\pi\beth^2}} \exp\left\{-\frac{(-x-\beth)^2}{2\beth^2}\right\}, \tag{41}$$

where $\aleph, \beth, \beth$ are parameters of regression, to the histogram data, the wanted channels are given by the $\beth$-parameter of the fit.

The fit was carried out using the python method `scipy.optimize.curve_fit`. We determined the data used for the fit in the following way: Because the energies correspond to the radioactive decays with the highest energies, the wanted peaks should be the ones found rightmost of each channel spectrum. As the function to be fitted is symmetric in the channels (cf. eq. (41)), we selected the data used by the fit by looking at the top of the peak and singling out the data points where the intersecting curve would roughly be symmetric. This is illustrated in fig. 16, where one can see that the data roughly below 2500 starts to become asymmetric in the channels. The result of the fits is shown alongside the reduced chi square in table 10; the corresponding plots can be found in the appendix (cf. figs. 52 to 54).

Based on the three energy peak locations characterized by the $\beth$-parameter one can carry out a linear regression in order to calibrate the detector by energy. Because the python module used for the following linear fit is based on a non-linear least squares model neglecting the $x$-error, the regression will be performed without

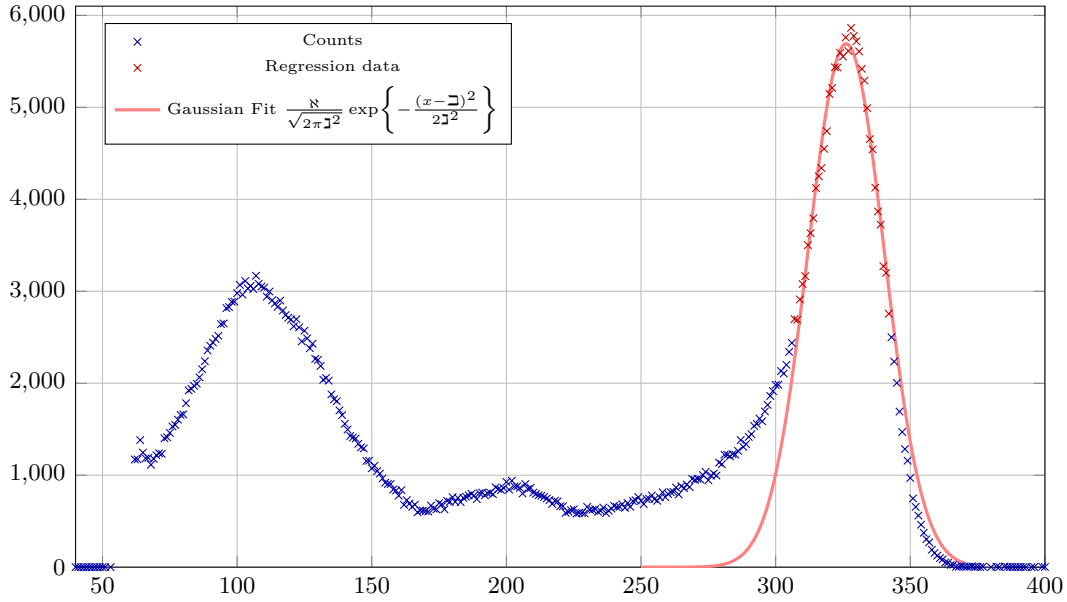


Figure 16: Background-subtracted counts of each MCA channel of the CdTe detector using the americum source. Additionally, the Gaussian fit of the peak is shown.

considering the uncertainty in ב. Now, by plotting the energy $E$ against ב and performing a fit of the form

$$E = ð \cdot ב + ſ\,, \tag{42}$$

where ð and ſ are parameters of regression, one is now able to identify a specific photon energy $E$ with the corresponding MCA channel ב. The data points for silicon can be seen in fig. 17 alongside the fit. Correspondingly, the plot for the CdTe detector can be found in the appendix (cf. fig. 51). The results from the linear fit is shown in table 10.

| Detector | ð/eV | ſ/eV |
|---|---|---|
| Silicon | $1.959\,092\,9 \pm 0.000\,000\,9 \times 10^{-1}$ | $-1.6171 \pm 0.0008$ |
| CdTe | $1.857\,073 \pm 0.000\,004 \times 10^{-1}$ | $-1.081 \pm 0.011$ |

Table 9: Results from the linear regression .

### 4.2.2 Determination of the Absorption Coefficient

In order to compare the absorption probabilities of both semiconductor detectors, the absorption ratio has to be calculated. For a given peak energy $E$, the absorption ratio $\eta_E$ is given by the ratio of the absorption probabilities of the detectors which in turn are proportional to the observed frequencies. In order to account for the difference in active area of both semiconductor detectors, the ratio $\eta_E$ is given by [3]

$$\eta_E = \frac{ℵ^E_{\mathrm{Si}}}{ℵ^E_{\mathrm{CdTe}}} \cdot \frac{a_{\mathrm{CdTe}}}{a_{\mathrm{Si}}}, \tag{43}$$

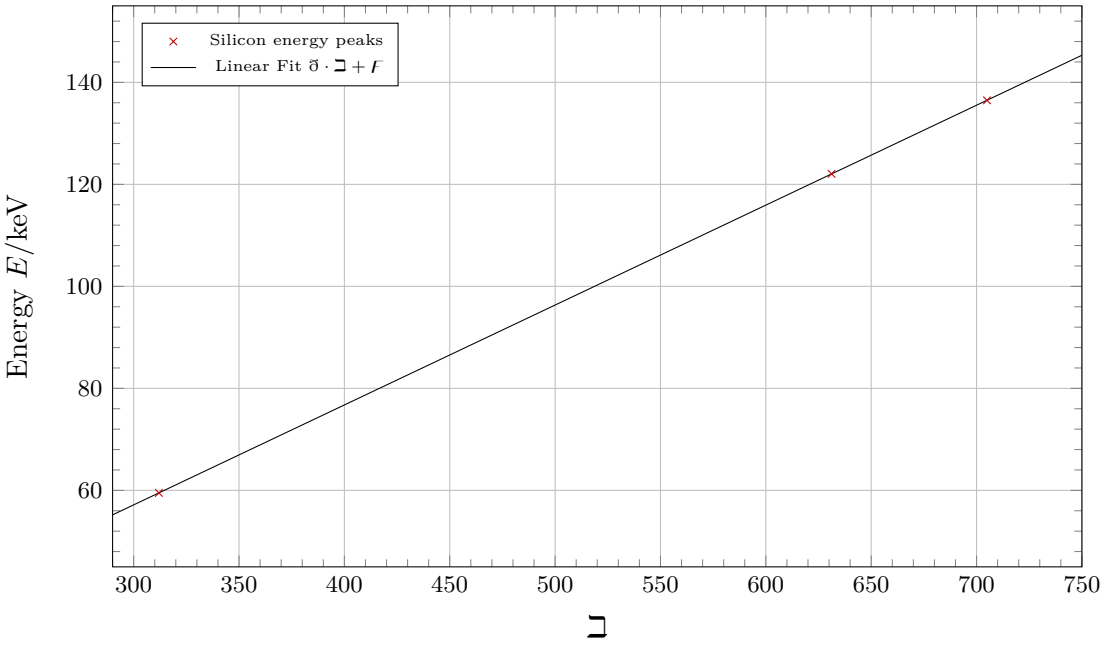


Figure 17: Linear regression in order to determine the energy conversion formula for silicon.

| Detector | Energy $E$/keV | א | ב/$10^2$ | ג/$10^1$ | $\chi^2_\nu$ |
|---|---|---|---|---|---|
| Silicon | 59.5 | $1.87 \pm 0.20 \times 10^4$ | $3.1197 \pm 0.0015$ | $1.238 \pm 0.013$ | 2.04 |
| | 122.06 | $7.80 \pm 0.10 \times 10^3$ | $6.321 \pm 0.017$ | $1.249 \pm 0.020$ | 1.04 |
| | 136.47 | $6.3 \pm 0.3 \times 10^2$ | $7.049 \pm 0.007$ | $1.24 \pm 0.09$ | $8.10 \times 10^{-1}$ |
| CdTe | 59.5 | $2.011 \pm 0.026 \times 10^5$ | $3.2618 \pm 0.0016$ | $1.409 \pm 0.023$ | 8.66 |
| | 122.06 | $2.57 \pm 0.06 \times 10^5$ | $6.6251 \pm 0.0020$ | $1.59 \pm 0.05$ | 4.56 |
| | 136.47 | $2.22 \pm 0.11 \times 10^4$ | $7.409 \pm 0.005$ | $1.63 \pm 0.09$ | 1.36 |

Table 10: Fit parameters determined by the python module for each of the radioactive sources and semiconductor detectors.

where the ℵ's are defined per table 10 and $a_{\mathrm{Si}} = 100\,\mathrm{mm}^2, a_{\mathrm{CdTe}} = 23\,\mathrm{mm}^2$ refer to the detectors active areas. Assuming the areas to be exact, the error on the absorption coefficient is given by Gaussian error propagation:

$$s_{\eta_E} = \frac{a_{\mathrm{CdTe}}}{a_{\mathrm{Si}}} \sqrt{\left(\frac{s_{\aleph^E_{\mathrm{Si}}}}{\aleph^E_{\mathrm{CdTe}}}\right)^2 + \left(\frac{\aleph^E_{\mathrm{Si}}}{\left(\aleph^E_{\mathrm{CdTe}}\right)^2} \cdot s_{\aleph^E_{\mathrm{CdTe}}}\right)^2}. \tag{44}$$

The absorption ratios are given in table 11 with their respective literature value.

| $E$/keV | $\eta_E$ | $\eta_E^{\mathrm{Lit}}$ |
|---|---|---|
| 59.5 | $2.14 \pm 0.03 \times 10^{-2}$ | $1.40 \times 10^{-2}$ |
| 122.06 | $6.98 \pm 0.19 \times 10^{-3}$ | $1.83 \times 10^{-2}$ |
| 136.47 | $6.5 \pm 0.4 \times 10^{-3}$ | $2.00 \times 10^{-2}$ |

Table 11: Absorption ratios of both semiconductor detectors for the peak energies with their respective literature value [3].

### 4.2.3 Determination of the Relative Energy Resolution

Lastly, the relative energy resolution $\mathcal{R}$ of each semiconductor detector is to be calculated for each peak energy. For a given energy $E$, the relative energy resolution is given by [3]

$$\mathcal{R} = 2\sqrt{2\log 2} \cdot \frac{\sigma}{E}, \tag{45}$$

where $\sigma$ is to be understood as the standard deviation of the Gaussian distribution belonging to an energy peak. As $\sigma$ and $E$ are linearly related to the channels as shown in section 4.2.1, the relative energy resolution can be calculated as

$$\mathcal{R} = 2\sqrt{2\log 2} \cdot \frac{\beth}{\daleth}. \tag{46}$$

By Gaussian error propagation one can calculate the error on the energy resolution:

$$s_{\mathcal{R}} = 2\sqrt{2\log 2}\sqrt{\left(\frac{s_\beth}{\daleth}\right)^2 + \left(\frac{\beth}{\daleth^2} \cdot s_\daleth\right)^2} \tag{47}$$

The relative energy resolutions for each semiconductor detector is shown in table 12.

| Detector | Energy $E$/keV | $\mathcal{R}$ |
|---|---|---|
| Silicon | 59.5 | $9.34 \pm 0.10 \times 10^{-2}$ |
| | 122.06 | $4.66 \pm 0.06 \times 10^{-2}$ |
| | 136.47 | $4.14 \pm 0.03 \times 10^{-2}$ |
| CdTe | 59.5 | $1.018 \pm 0.017 \times 10^{-1}$ |
| | 122.06 | $5.66 \pm 0.16 \times 10^{-2}$ |
| | 136.47 | $5.10 \pm 0.29 \times 10^{-2}$ |

Table 12: Energy resolutions of each semiconductor at each peak energy.

### 4.3 Discussion

In the third part of the experiment, a linear regression was carried out on data determined by a fit in order to calibrate the energy measurements of both of the semiconductor detectors (cf. section 4.2.1). The fit results are given in table 9. Immediately conspicuous is the relatively low error on the parameters returned by the fit. Although the linearity between channels and energy values seems strongly linear by visual judgement (as illustrated in figs. 17 and 51), we suspect the errors on the fit parameters to be faulty. Taking further into account that the regression was performed on data sets featuring only three data pairs each, we conclude that while the regression seems to confirm a linear relationship to a reasonably high degree, the error given on the parameters is misleading at best.

Although not directly related to the low error on the fit parameters of the energy calibration, one thing that seems striking is the quality of the Gaussian fits shown exemplarily in fig. 16: As one can see in the figure, the right half of the curve runs above the data points not used for the fit. As we are dealing with non-negative frequences within a histogram, it seems improbable that the Gaussian fit actually fits the data. This may be due to the fact that not every distribution encountered in radioactive decays can be modeled by a Gaussian curve, but rather their limiting distribution as the amount of observations approach infinity. For example, for the data shown in fig. 16, a binomial distribution may be more suitable.

Next to the determination of the parameters on the energy calibration, the absorption ratios of the semiconductor detectors were calculated (cf. section 4.2.2). As one can see in table 11 where our results are shown alongside their respective literature value, our results don't fit the expected values at all: The deviations between the result and the literature value range from $24\sigma$ up to a $64\sigma$-environment. The discrepancy doesn't seem to be due to a simple scaling error, as our results don't even fit the trend given by the literature value. This leads us to think that there exists a grave systematic error underlying our measurements. As the absorption measurements depend on the $\aleph$-parameter (which is defined per eq. (41)) corresponding to the amplitude of the peak, it seems that the cause of the systematic error lies in the amplitude of the intensity distribution[2]. Similar to the last part, this may be due to the Gaussian distribution not fitting the data.

However, we think that the fault may lie in the quality of the experiment's setup: If the radioactive sources are past several half-lives, the condition of the bad intensity distribution is exacerbated. As $^{57}$Co has a half-live of about 271 d, it may very well be possible that the source used was already depleted to some degree. This argumentation doesn't go well with Americum, as the $^{241}$Am isotope's half-live amounts to 432 a.

Lastly, the relative energy resolutions were determined for each peak energy for both of the semiconductors (cf. table 12). Comparing the resolutions for each energy across both detectors, we note that the CdTe detector's resolution is slightly higher than that of the silicon detector. As the relative energy resolution is a measure of the detectors accuracy, our results seem to hint that the CdTe detector is slightly

[2] As we already established in section 4.2.1, the channel-energy relationship seems to be mostly linear, meaning that peak positions seem to be consistent.

more accurate than the silicon diode. However, more noticeable is the fact that the 59.5 keV peak yields double the resolution of the other energy peaks, implying the possibility that the sources may be of different qualities. Furthermore, even only considering the Cobalt source, the resolutions differ by up to a range of $17\sigma$, hinting at inconsistencies in our measurements.

Many of the uncertainties discussed above can be improved by significantly longer measurement times and the use of comparable radioactive sources.

# A Appendix

## A.1 Figures and Tables

| Semiconductor | Angle | $\aleph/\frac{1}{\circ}$ | ב | ג/$\frac{1}{\circ}$ | ד |
|---|---|---|---|---|---|
| Germanium | positive | $-0.050 \pm 0.006$ | $1.82 \pm 0.18$ | $0.086 \pm 0.009$ | $-2.58 \pm 0.29$ |
| | negative | $0.044 \pm 0.007$ | $1.67 \pm 0.21$ | $-0.080 \pm 0.004$ | $-2.57 \pm 0.14$ |
| Silicon | positive | $-0.153 \pm 0.007$ | $7.1 \pm 0.3$ | $0.062 \pm 0.004$ | $-2.32 \pm 0.17$ |
| | negative | $0.157 \pm 0.009$ | $7.3 \pm 0.4$ | $-0.0590 \pm 0.0012$ | $-2.27 \pm 0.05$ |

Table 13: Regression parameters of the analysis of part 1.

| Semiconductor | Angle | $(\chi^2)_\mathfrak{t}$ | $(\chi^2_\nu)_\mathfrak{t}$ | $(\chi^2)_\mathfrak{a}$ | $(\chi^2_\nu)_\mathfrak{a}$ |
|---|---|---|---|---|---|
| Germanium | positive | $2.14 \times 10^1$ | 1.78 | $1.02 \times 10^1$ | $9.25 \times 10^{-1}$ |
| | negative | $2.78 \times 10^1$ | 2.32 | 6.30 | $4.20 \times 10^{-1}$ |
| Silicon | positive | $1.13 \times 10^2$ | 4.92 | $3.63 \times 10^2$ | $2.13 \times 10^1$ |
| | negative | $7.25 \times 10^1$ | 3.82 | $5.16 \times 10^1$ | 2.46 |

Table 14: Chi square alongside reduced chi square in order to quantify the goodness of the fits given by the parameters in table 13.

| Semiconductor | Angle | $\phi_\mathrm{g}/^\circ$ | $E_\mathrm{g}$/eV | $s^\mathrm{sys}_{E_\mathrm{g}}$/eV |
|---|---|---|---|---|
| Germanium | positive | $35.2 \pm 1.9$ | $6.5 \pm 0.3 \times 10^{-1}$ | $4.77 \times 10^{-5}$ |
| | negative | $-35.9 \pm 1.8$ | $6.4 \pm 0.2 \times 10^{-1}$ | $4.75 \times 10^{-5}$ |
| Silicon | positive | $44.0 \pm 1.6$ | $1.08 \pm 0.03$ | $4.40 \times 10^{-5}$ |
| | negative | $-44.1 \pm 1.3$ | $1.08 \pm 0.03$ | $4.40 \times 10^{-5}$ |

Table 15: Band gap energies and corresponding angles determined by our measurements of silicon and germanium.

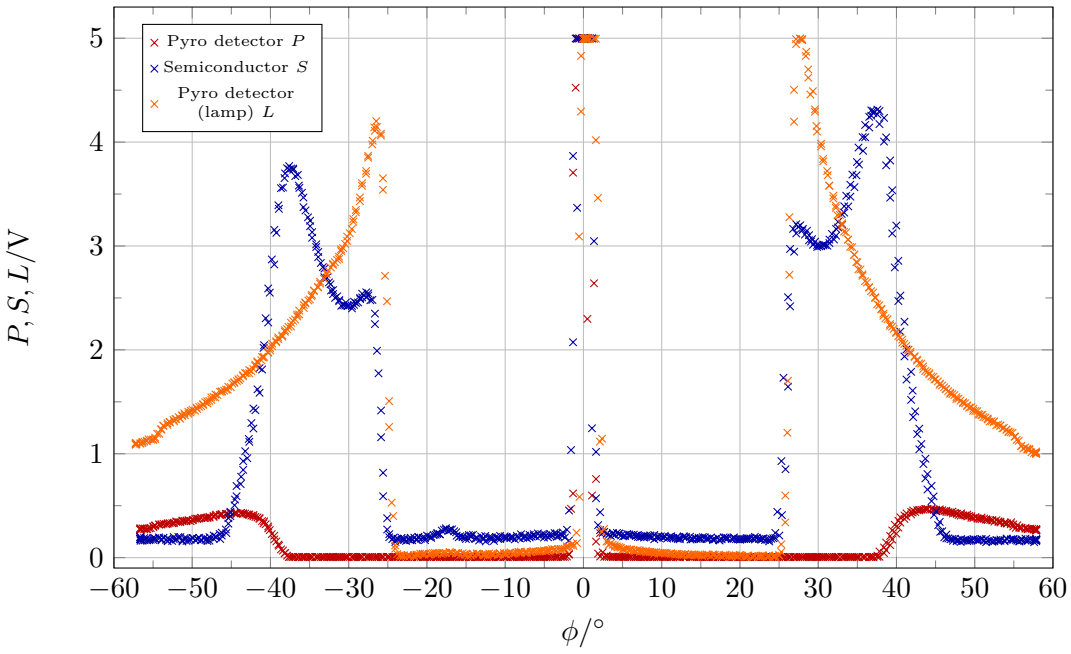


Figure 18: Main measurement and lamp measurement of the silicon semiconductor. The slight bump in the sample measurement can also be seen in the background measurement (cf. fig. 20).

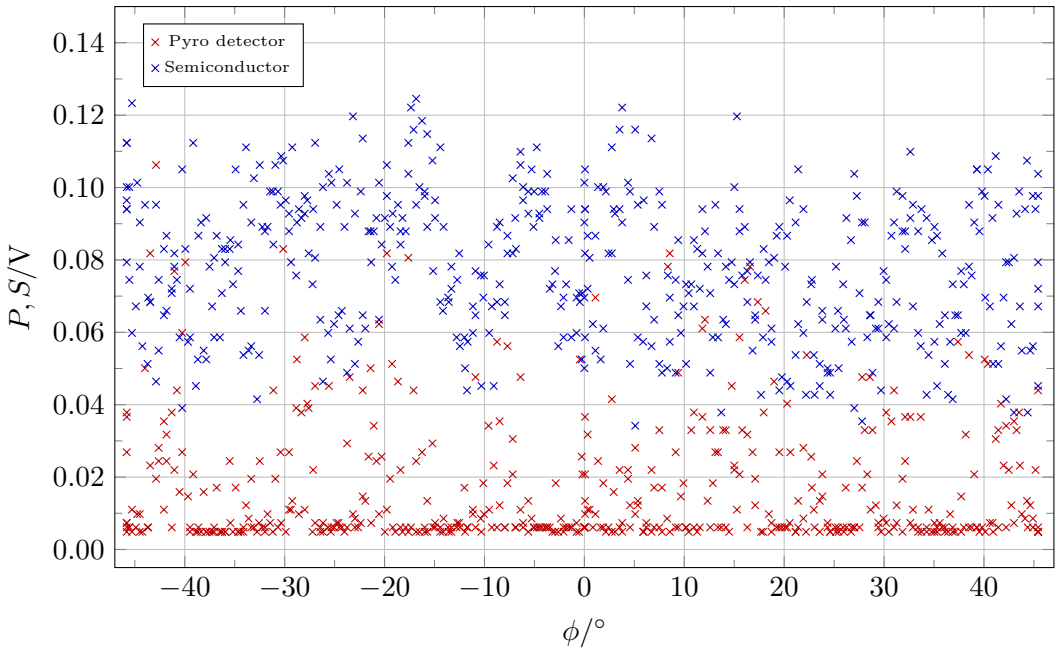


Figure 19: Background of the germanium sample measurement of part 1. As we think the data isn't dependent on the angle $\phi$ but is rather uniformly distributed, this measurement isn't considered in the analysis.

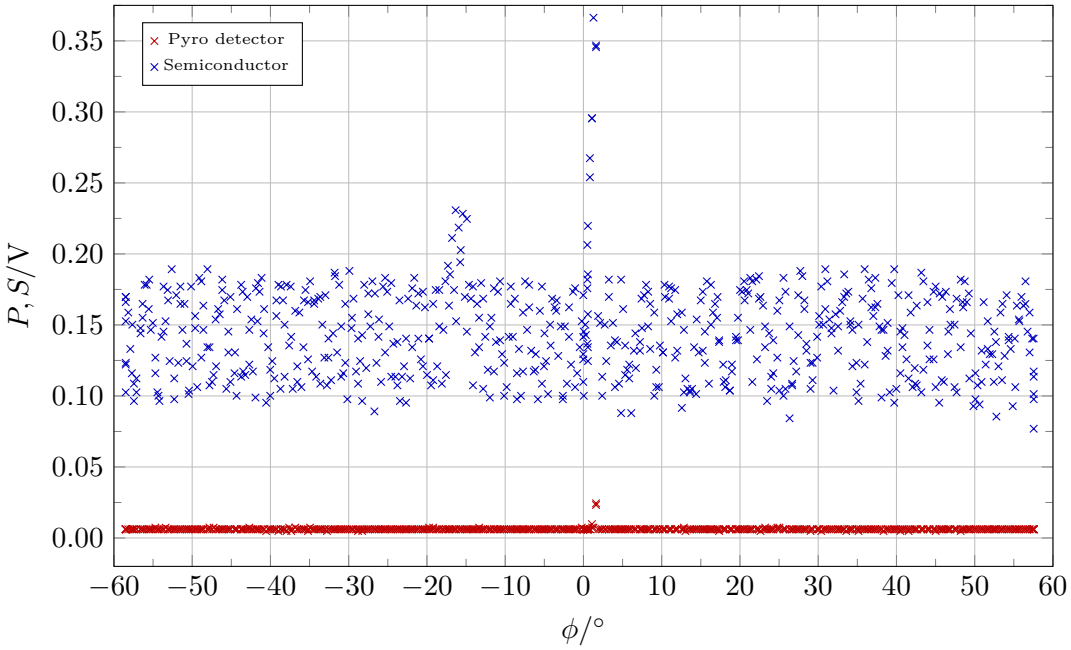


Figure 20: Background of the silicon sample measurement of part 1. Except for a bump at about −17° and the main peak in the middle, the data shown here is also mostly uniform. The main peak may be due to the aperture not being closed properly, while the left bump could stem from a reflection bypassing the aperture. As this effect isn't in the critical region, this series wasn't considered for the analysis, too.

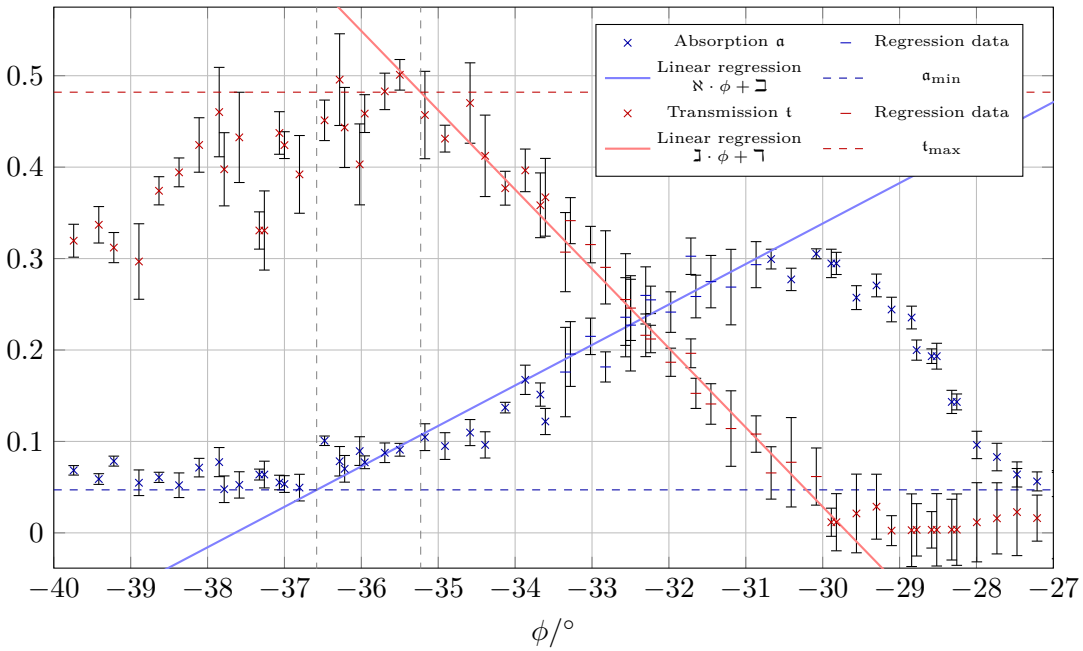


Figure 21: Plot of the absorption $\mathfrak{a}$ and transmission $\mathfrak{t}$ of the negative angle range of the germanium sample. Also shown is a linear regression with values given in eq. (9) as well as the intersection angles. The $\chi^2$ values are given in table 14.

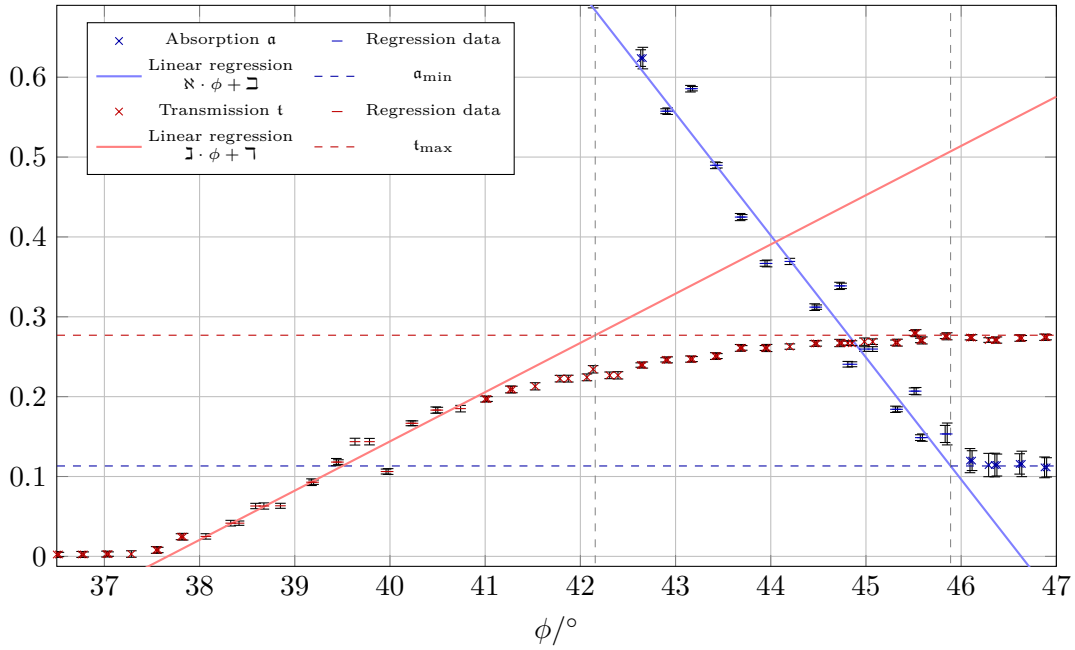


Figure 22: Plot of the absorption $\mathfrak{a}$ and transmission $\mathfrak{t}$ of the positive angle range of the silicon sample. Also shown is a linear regression with values given in eq. (9) as well as the intersection angles. The $\chi^2$ values are given in table 14.

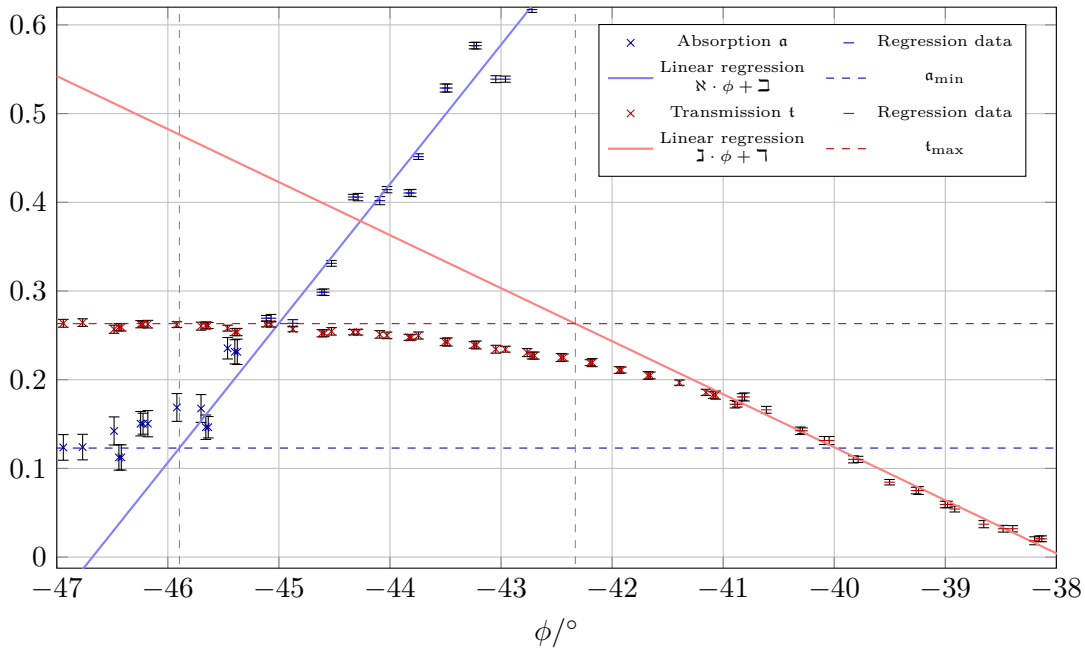


Figure 23: Plot of the absorption $\mathfrak{a}$ and transmission $\mathfrak{t}$ of the negative angle range of the silicon sample. Also shown is a linear regression with values given in eq. (9) as well as the intersection angles. The $\chi^2$ values are given in table 14.

| $d$/mm | $A$/V s | $\sigma$/s | $xc$/s |
|---|---|---|---|
| 2.01 | $2.459 \pm 0.005 \times 10^{-7}$ | $6.393 \pm 0.016 \times 10^{-7}$ | $5.0458 \pm 0.0015 \times 10^{-6}$ |
| 3.00 | $1.335 \pm 0.005 \times 10^{-7}$ | $6.96 \pm 0.03 \times 10^{-7}$ | $6.979 \pm 0.003 \times 10^{-6}$ |
| 4.02 | $8.24 \pm 0.08 \times 10^{-8}$ | $7.86 \pm 0.10 \times 10^{-7}$ | $8.876 \pm 0.009 \times 10^{-6}$ |
| 5.01 | $8.19 \pm 0.16 \times 10^{-8}$ | $10.0 \pm 0.2 \times 10^{-7}$ | $1.0858 \pm 0.0016 \times 10^{-5}$ |

Table 16: Fit parameters of the Gaussian fits of the first series of measurement by varying the distance.

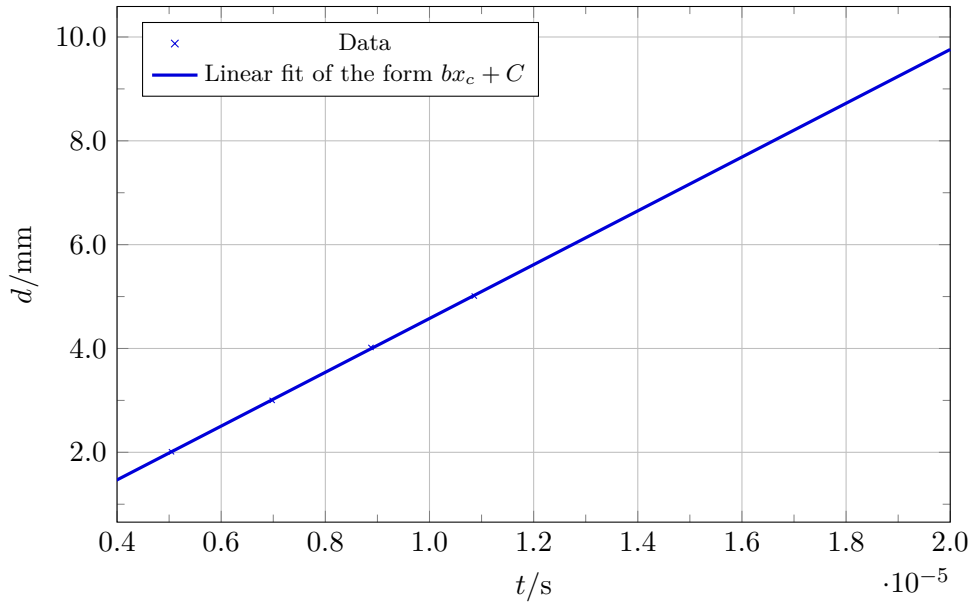


Figure 24: Linear fit of the form $d = b \cdot x_c + c$ to determine $\mu$. First series of measurements.

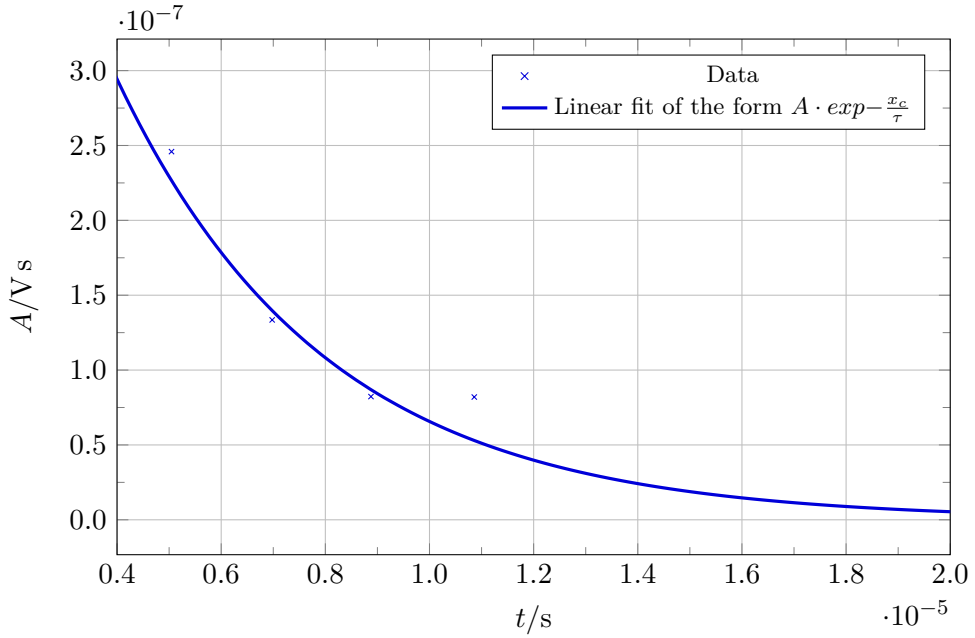


Figure 25: Exponential fit of the form $A = b \cdot e^{-\frac{x_c}{\tau}}$ to determine $\tau$. First measurements.

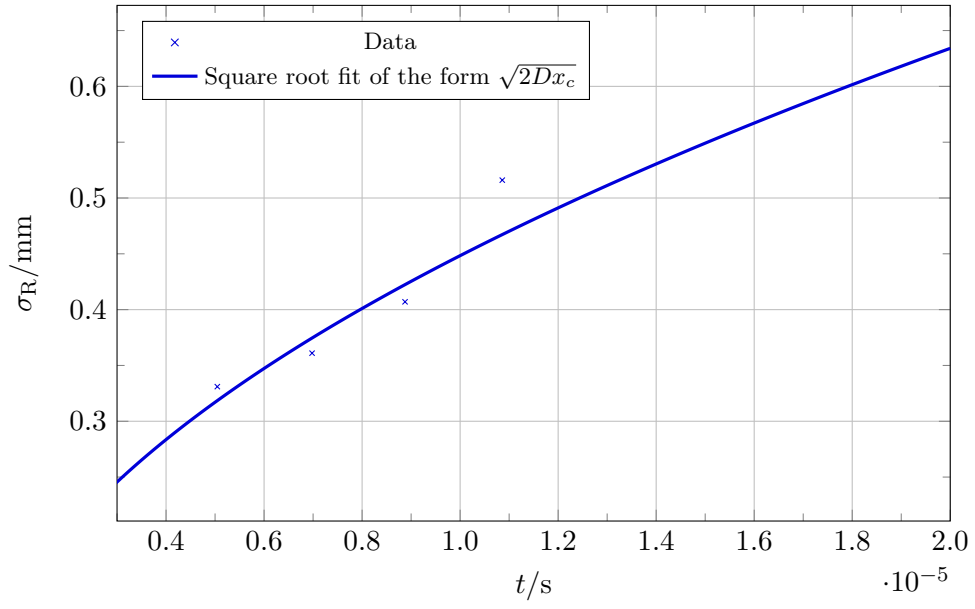


Figure 26: Square root fit of the form $\sigma_\mathrm{R} = \sqrt{2Dx_c}$ to determine $D$. First series of measurements.

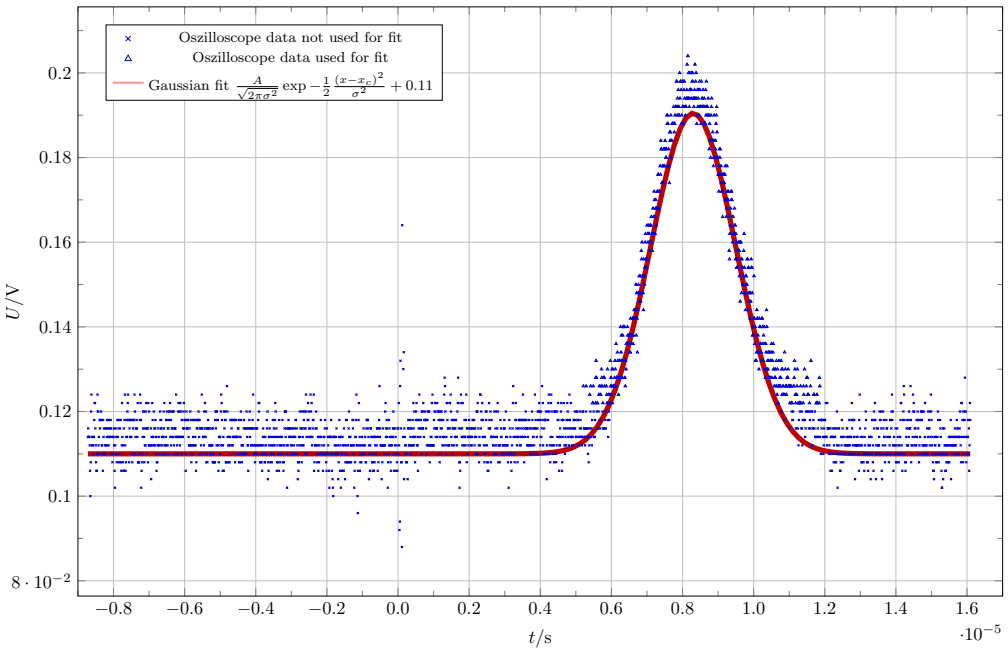


Figure 27: Measurement with the distance $d = 1.99\,\mathrm{mm}$ with $\chi^2_\nu = 5.96$.

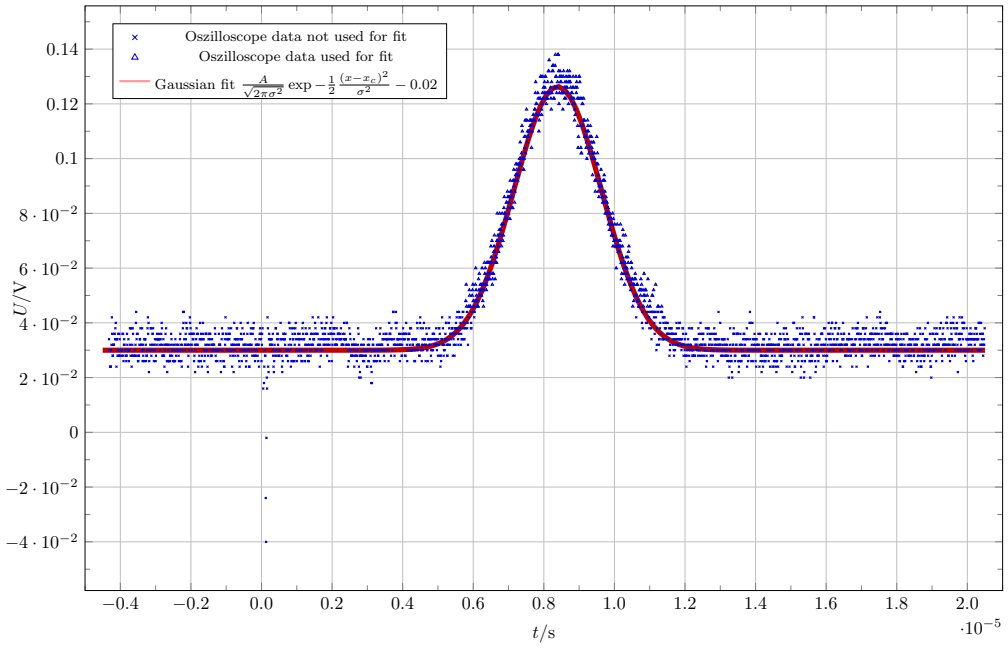


Figure 28: Measurement with the distance $d = 2.50\,\mathrm{mm}$ with $\chi^2_\nu = 6.00$.

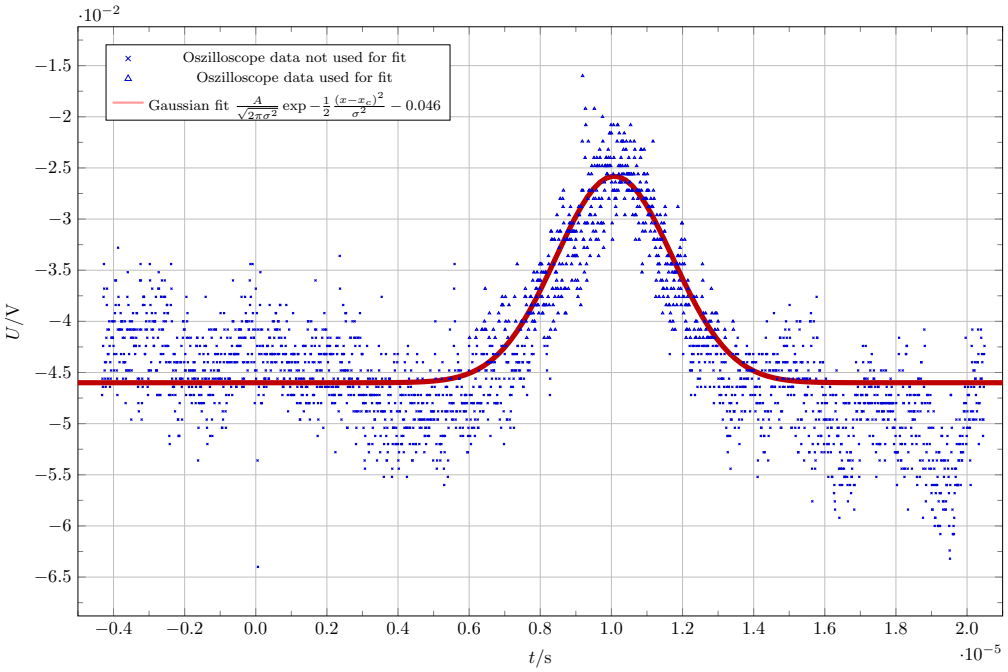


Figure 29: Measurement with the distance $d = 3.00\,\mathrm{mm}$ with $\chi^2_\nu = 2.63$.

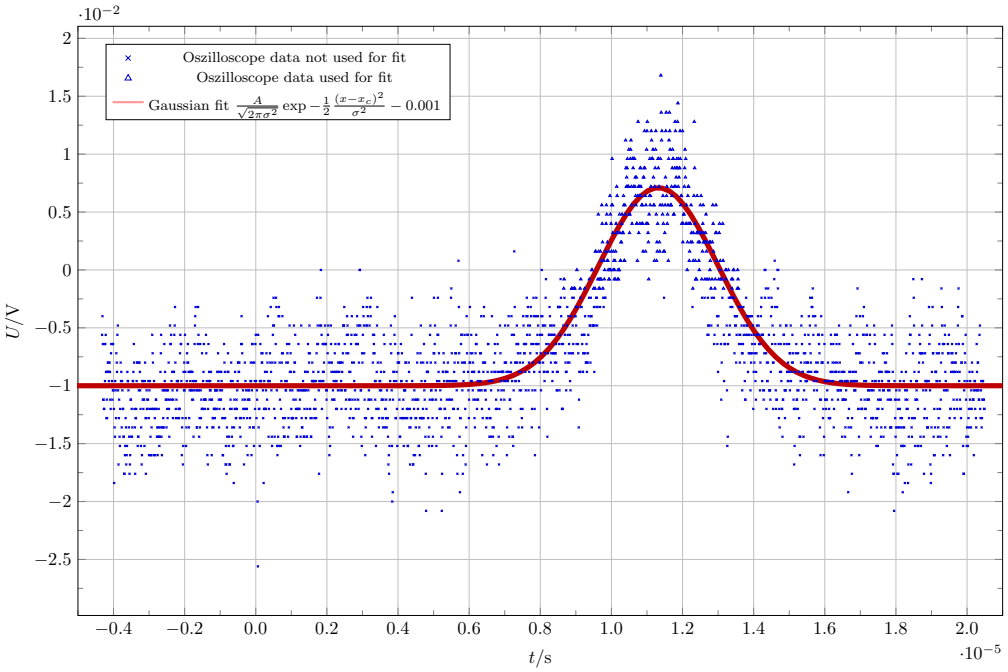


Figure 30: Measurement with the distance $d = 3.49\,\mathrm{mm}$ with $\chi^2_\nu = 2.24$.

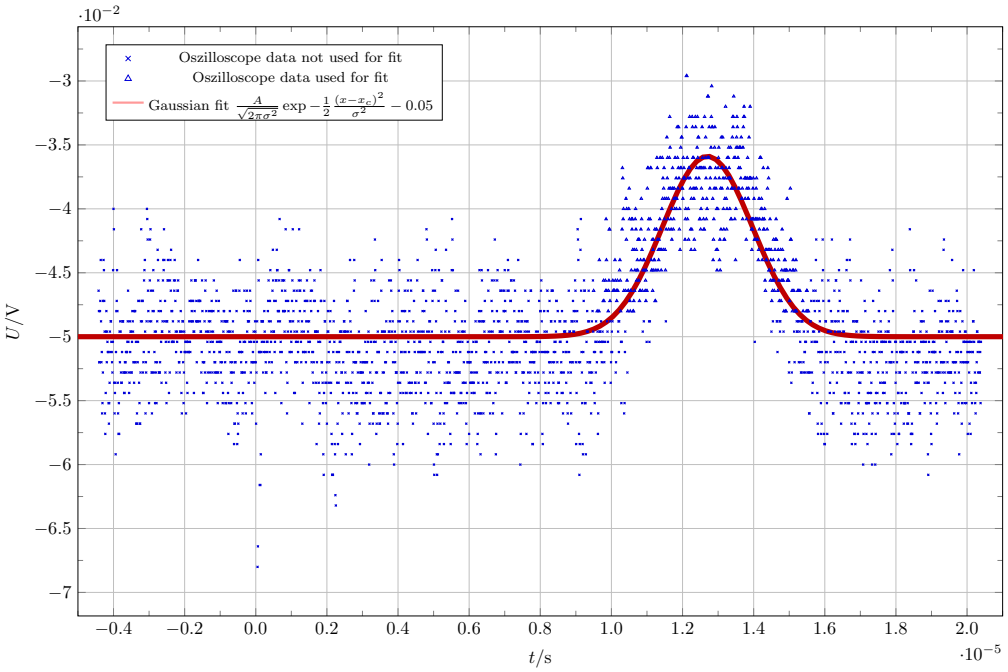


Figure 31: Measurement with the distance $d = 4.01\,\text{mm}$ with $\chi^2_\nu = 2.20$.

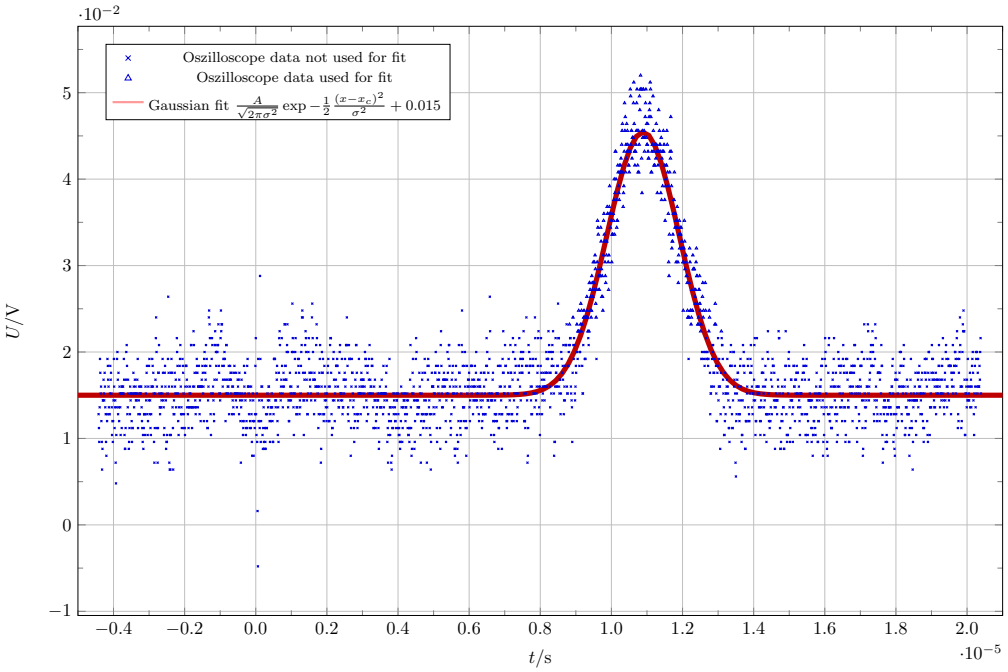


Figure 32: Measurement with the distance $d = 5.00\,\text{mm}$ with $\chi^2_\nu = 2.37$.

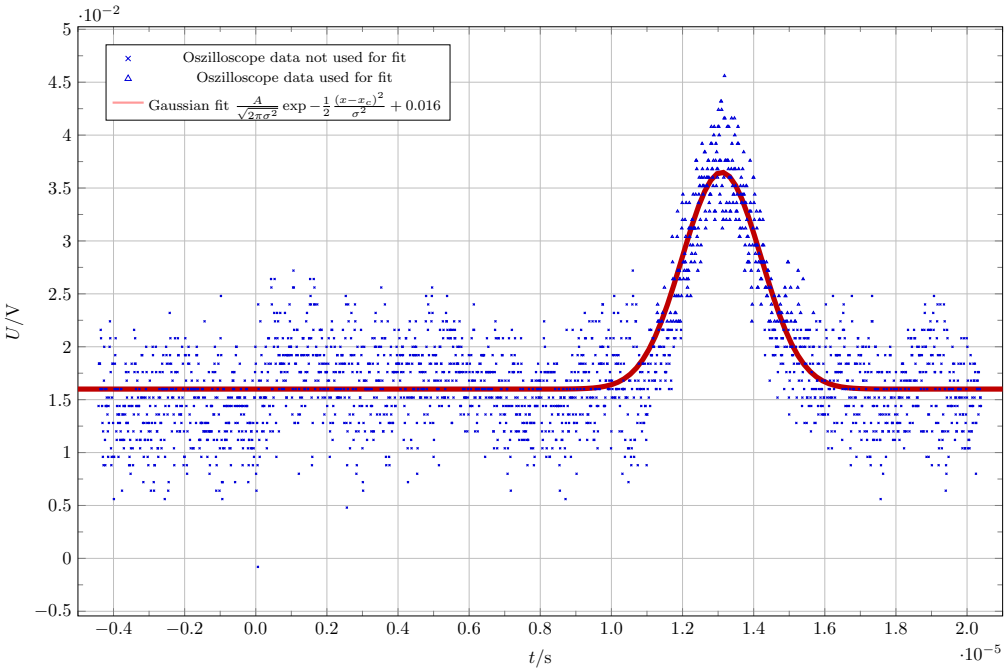


Figure 33: Measurement with the distance $d = 6.00\,\mathrm{mm}$ with $\chi^2_\nu = 2.46$.

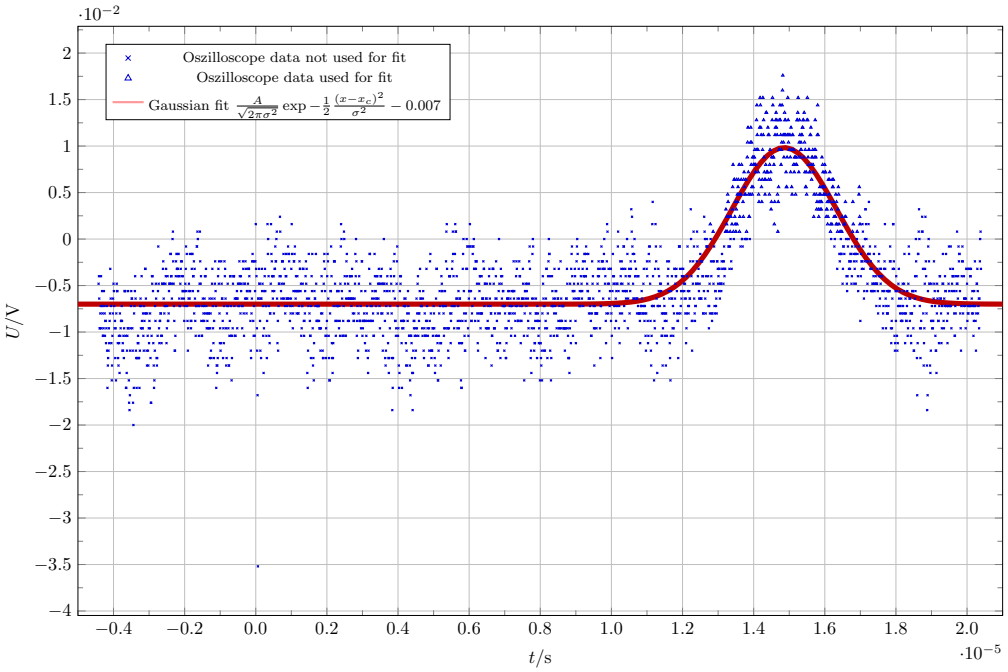


Figure 34: Measurement with the distance $d = 7.00\,\mathrm{mm}$ with $\chi^2_\nu = 2.03$.

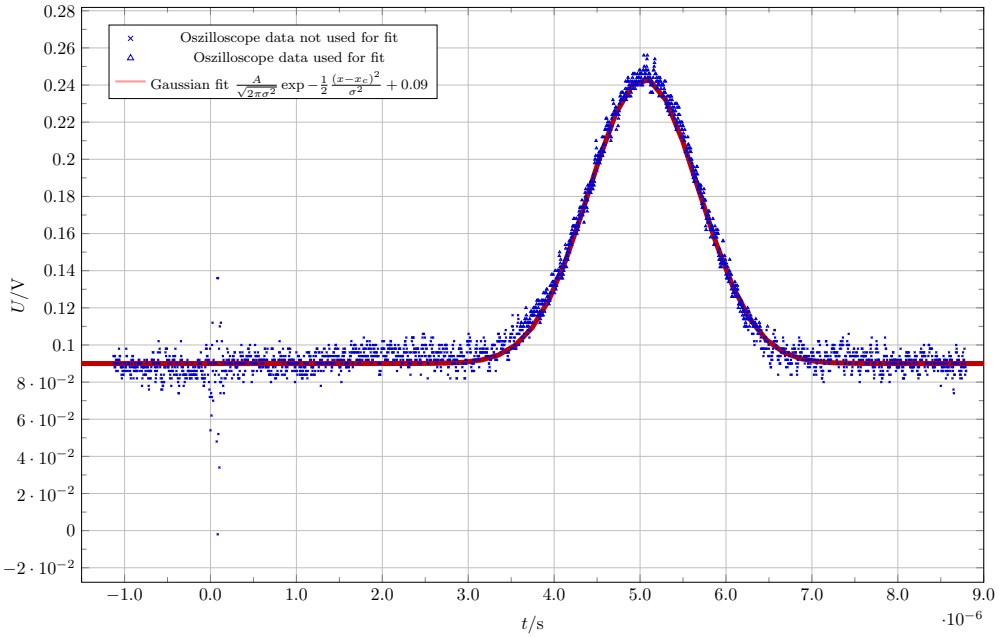


Figure 35: Measurement with the distance $d = 2.01\,\text{mm}$ with $\chi^2_\nu = 4.07$.

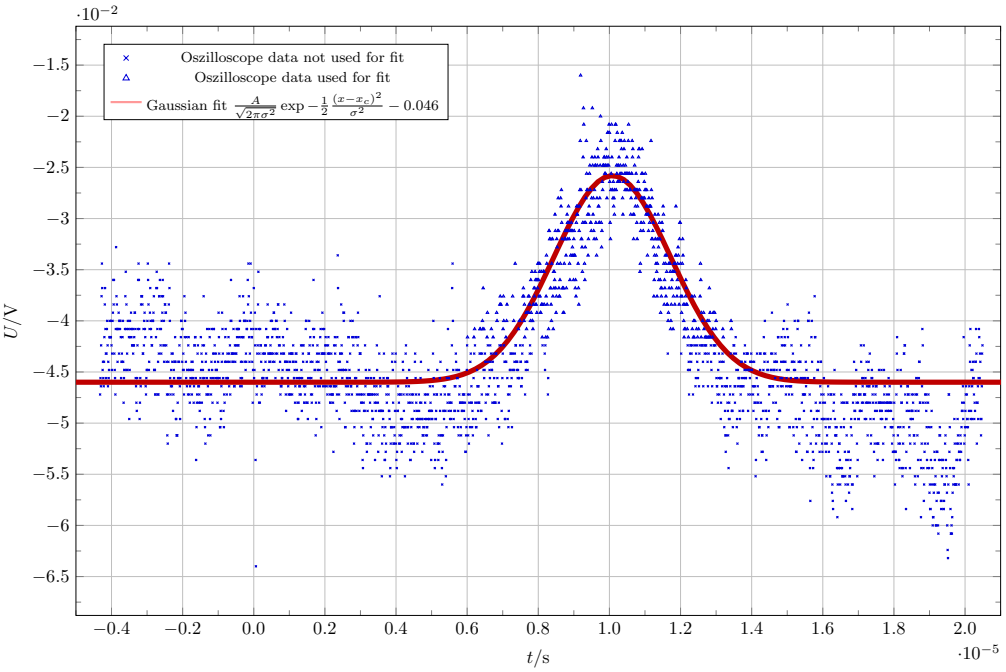


Figure 36: Measurement with the distance $d = 3.00\,\text{mm}$ with $\chi^2_\nu = 3.77$.

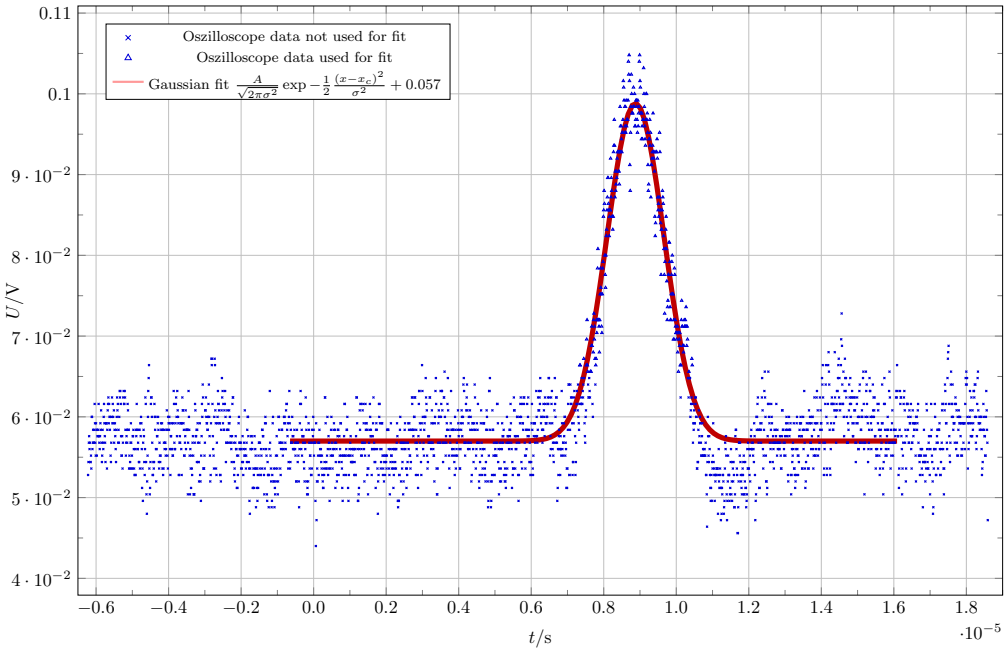


Figure 37: Measurement with the distance $d = 4.02\,\mathrm{mm}$ with $\chi^2_\nu = 3.14$.

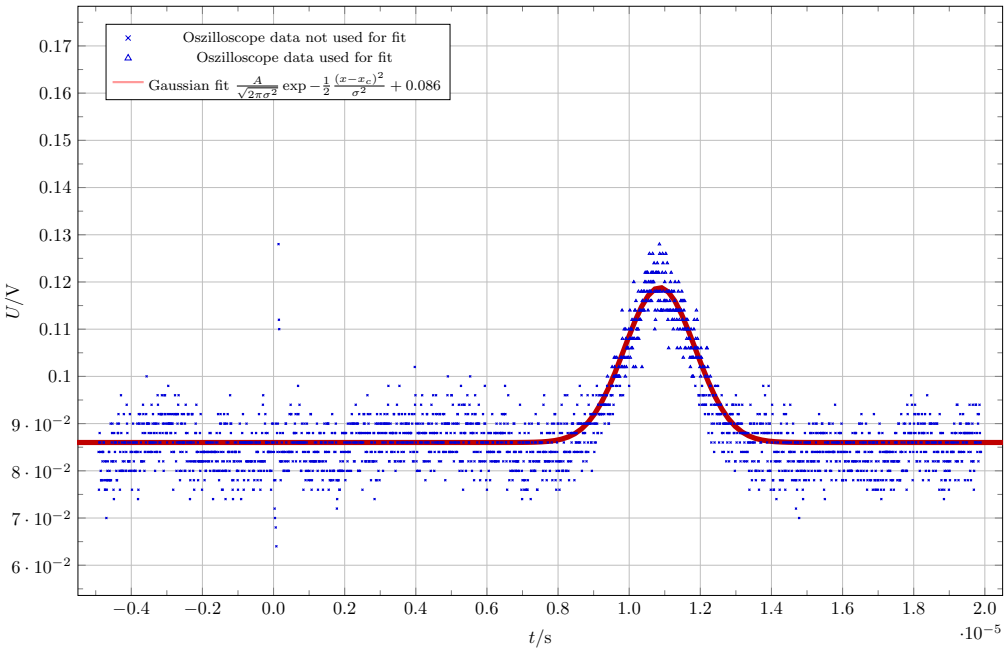


Figure 38: Measurement with the distance $d = 5.01\,\mathrm{mm}$ with $\chi^2_\nu = 3.85$.

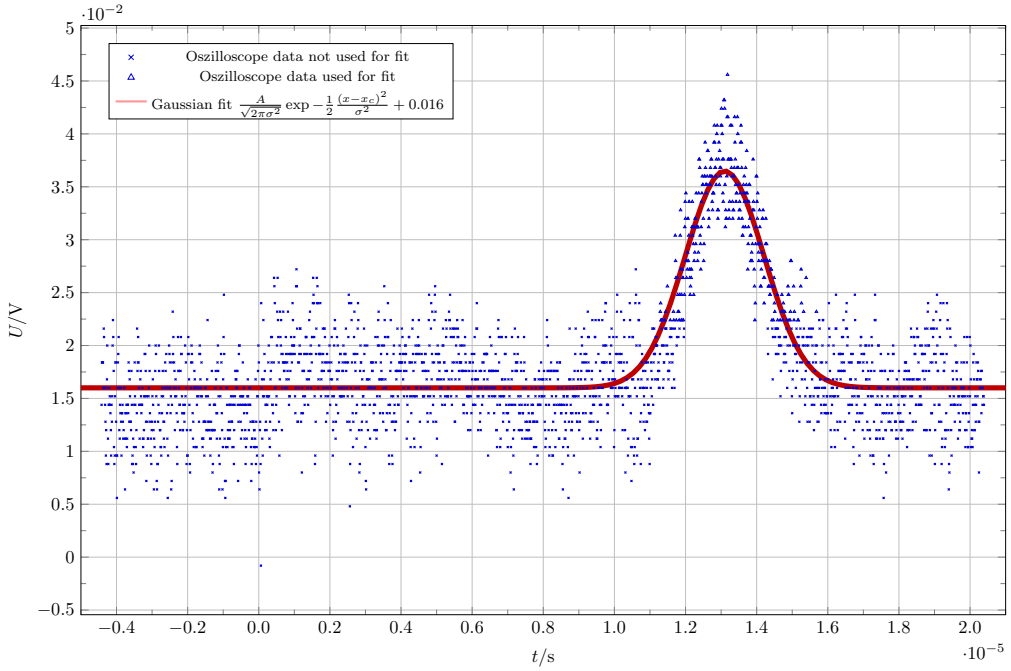


Figure 39: Measurement with the distance $d = 6.00\,\mathrm{mm}$, with a signal too weak to be fitted.

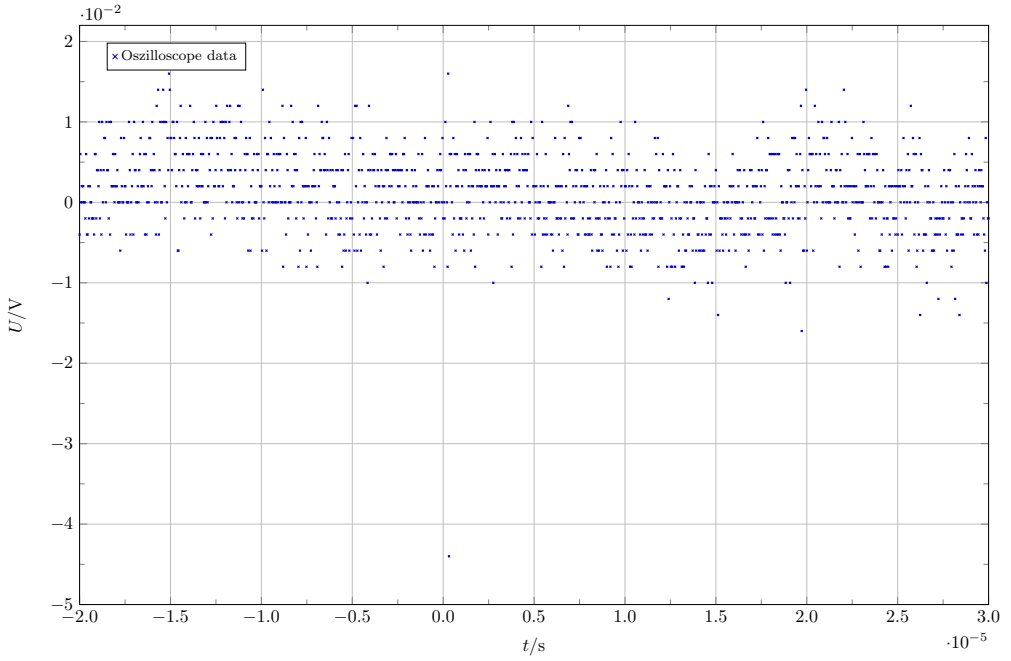


Figure 40: Measurement with the distance $d = 7.01\,\mathrm{mm}$, with a signal too weak to be fitted.

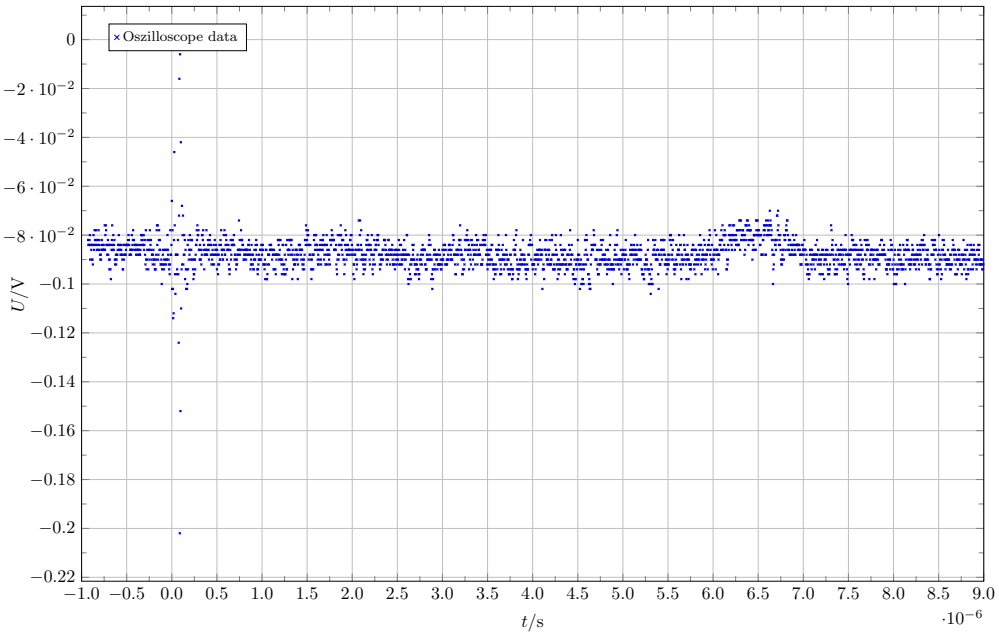


Figure 41: Measurement with the distance $d = 8.00\,\text{mm}$, with a signal too weak to be fitted.

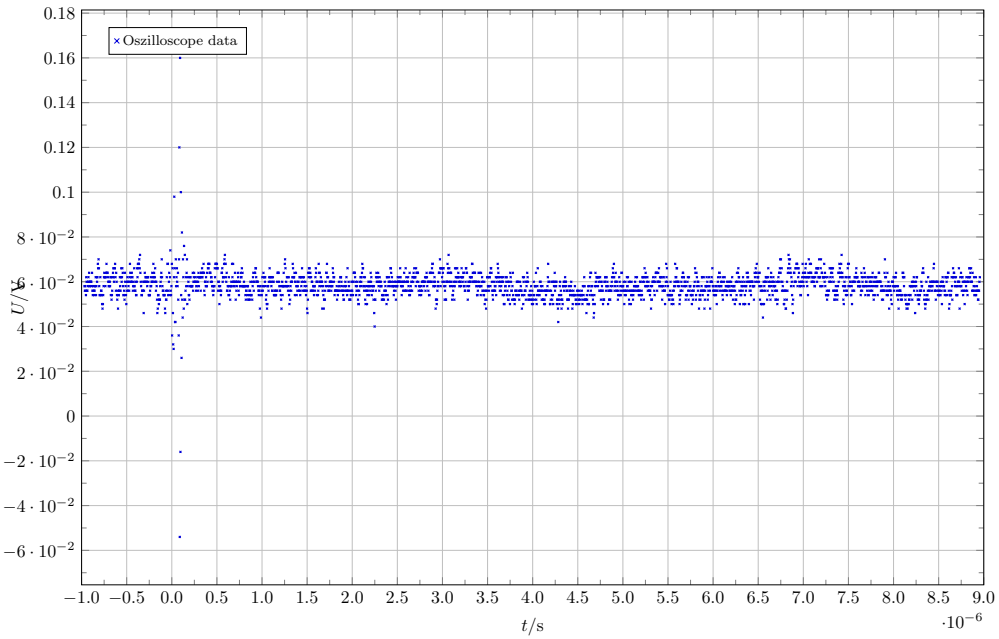


Figure 42: Measurement with the distance $d = 9.01\,\text{mm}$, with a signal too weak to be fitted.

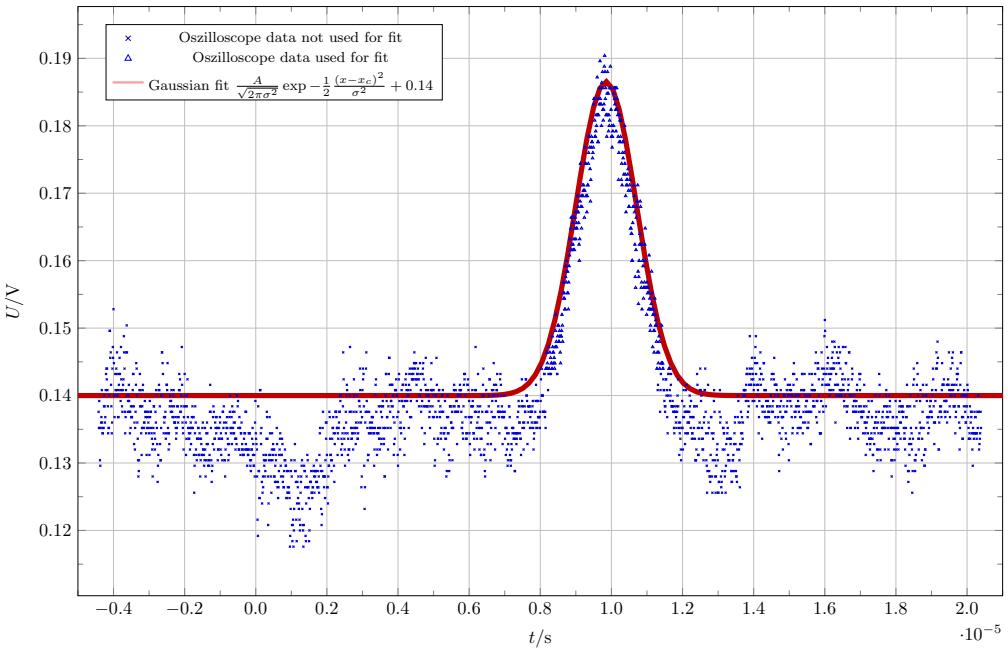


Figure 43: Measurement with the voltage $U = 49.6\,\mathrm{V}$ with $\chi^2_\nu = 2.75$.

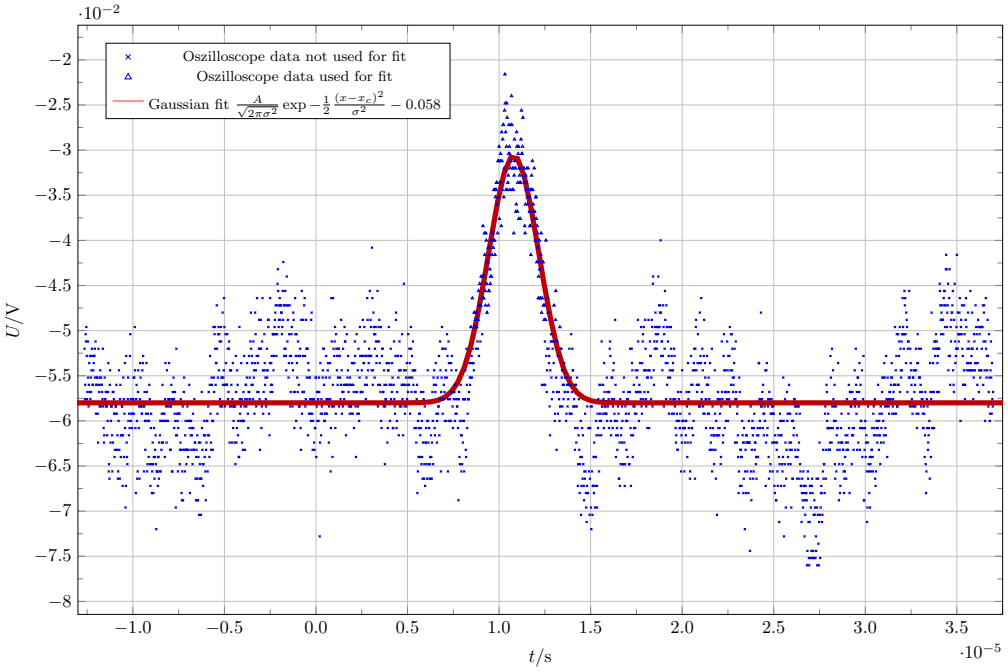


Figure 44: Measurement with the voltage $U = 44.8\,\mathrm{V}$ with $\chi^2_\nu = 2.74$.

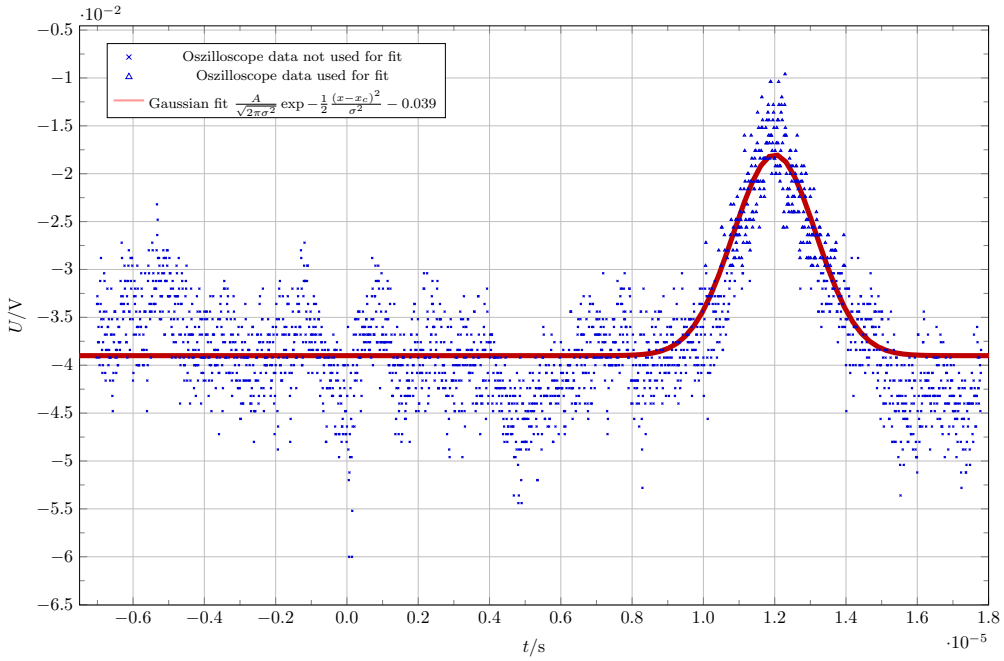


Figure 45: Measurement with the voltage $U = 40.0\,\mathrm{V}$ with $\chi^2_\nu = 2.67$.

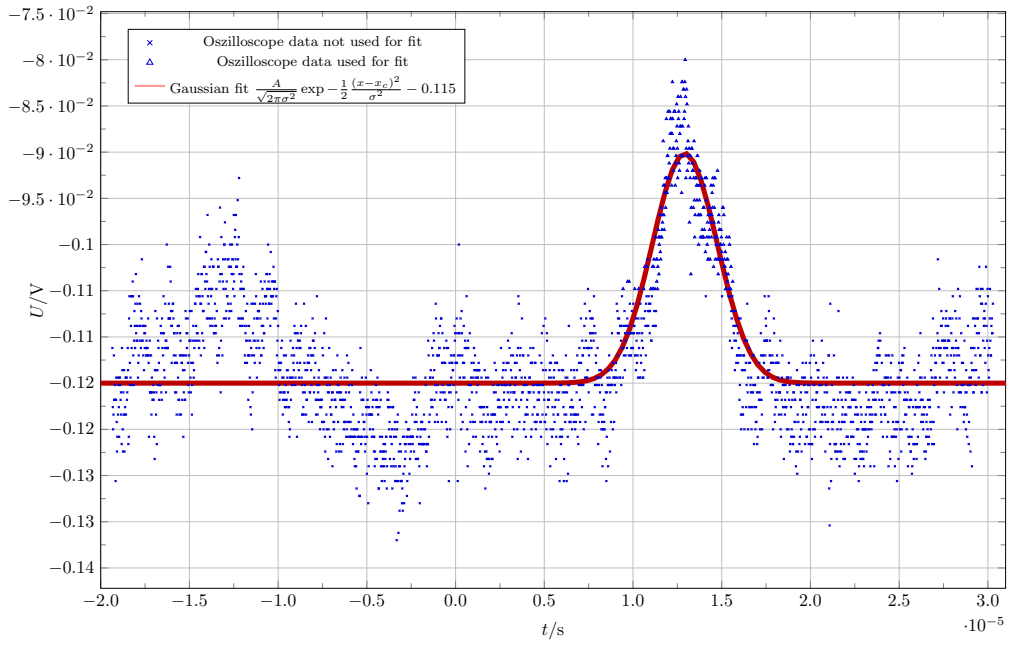


Figure 46: Measurement with the voltage $U = 35.2\,\mathrm{V}$ with $\chi^2_\nu = 3.91$.

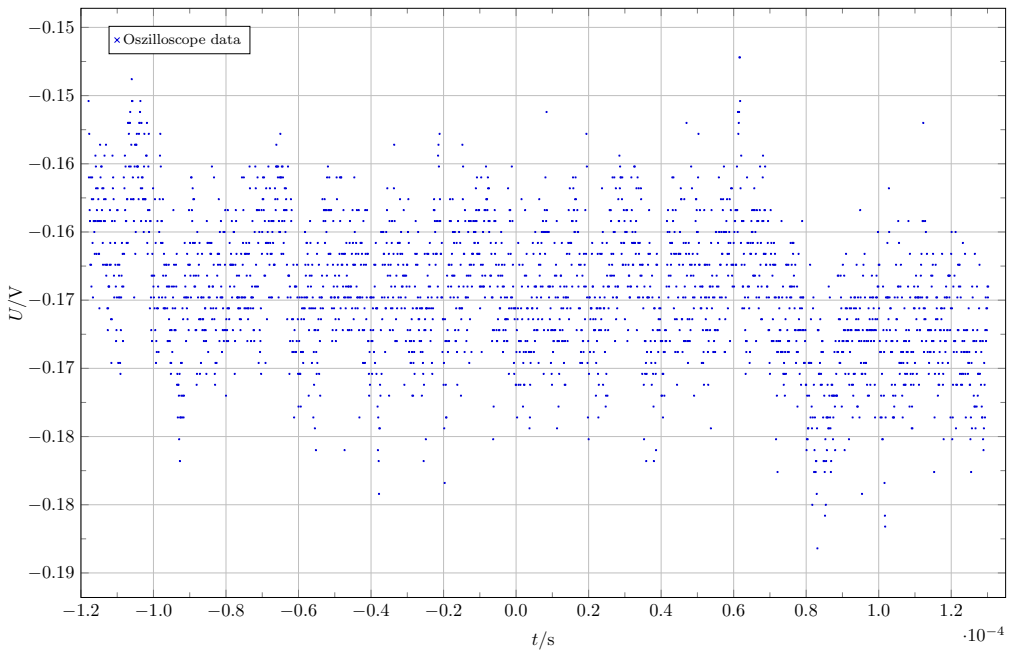


Figure 47: Measurement with the voltage $U = 30.0\,\mathrm{V}$ with a signal too weak to be fitted.

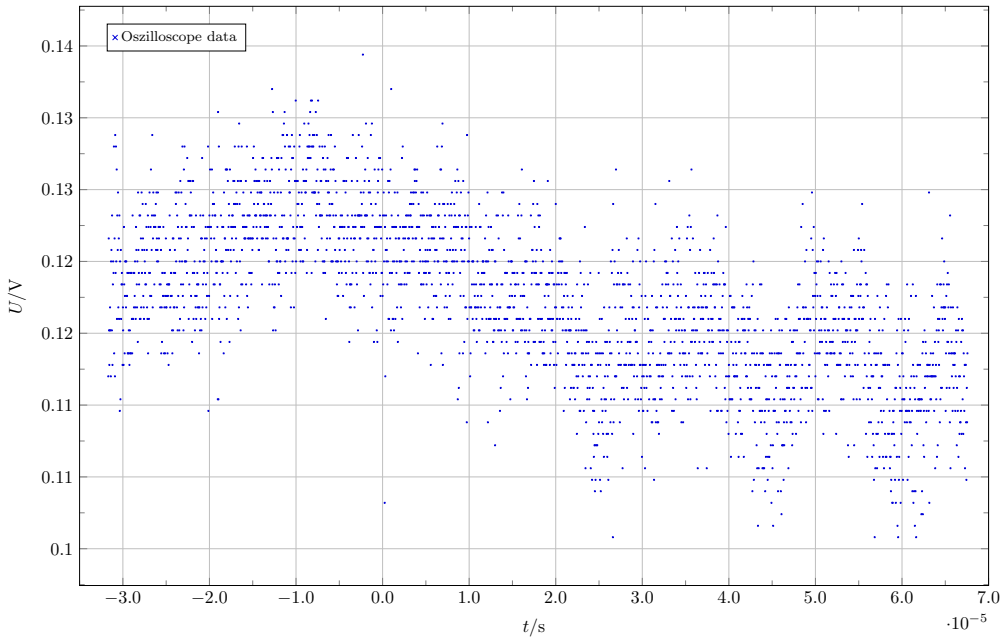


Figure 48: Measurement with the voltage $U = 24.8\,\mathrm{V}$ with a signal too weak to be fitted.

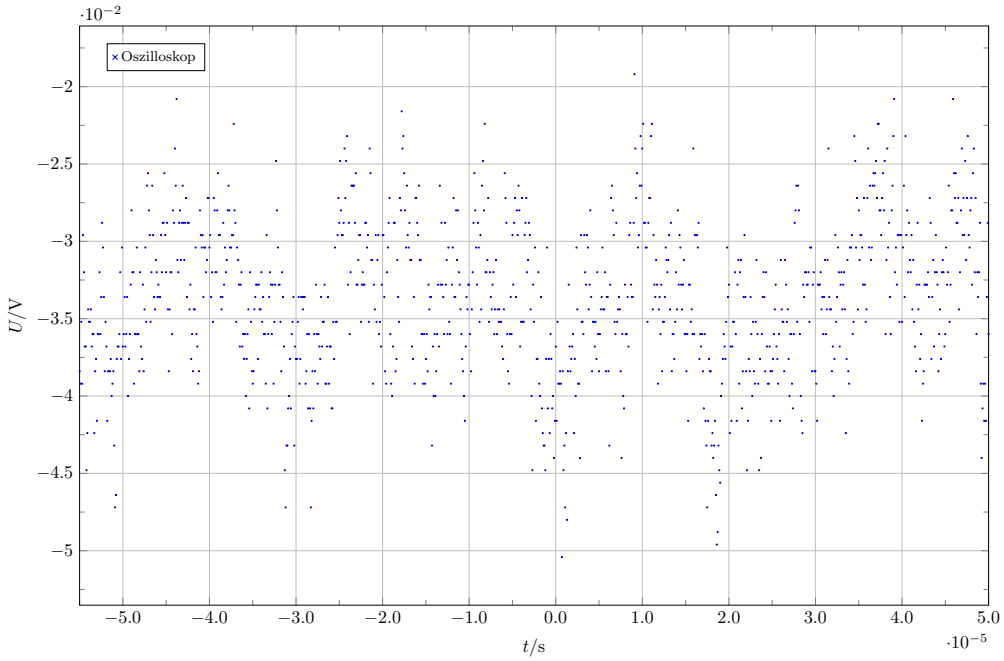


Figure 49: Measurement with the voltage $U = 20.0\,\mathrm{V}$ with a signal too weak to be fitted.

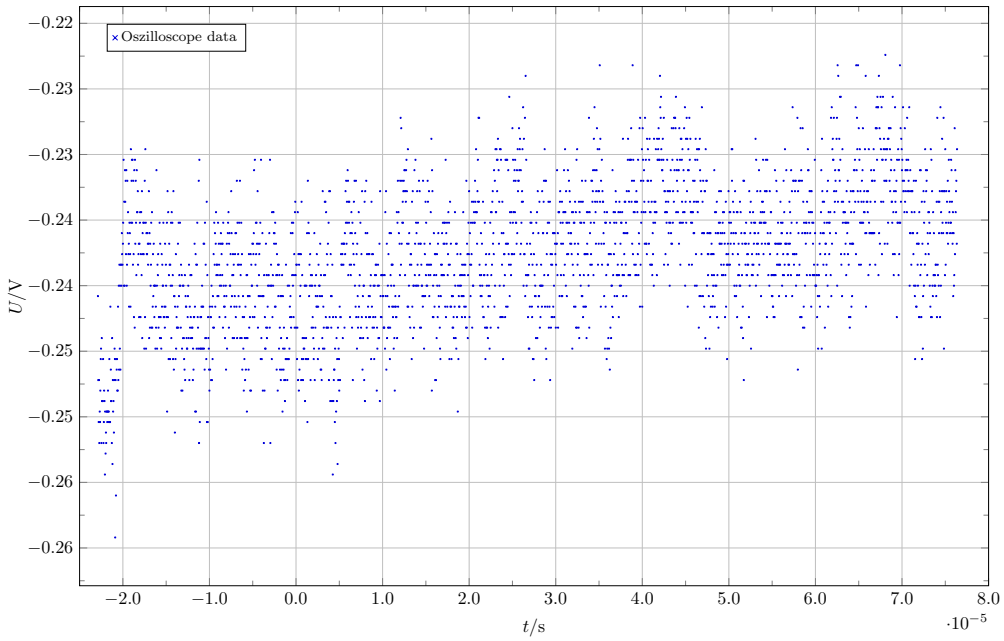


Figure 50: Measurement with the voltage $U = 15.2\,\mathrm{V}$ with a signal too weak to be fitted.

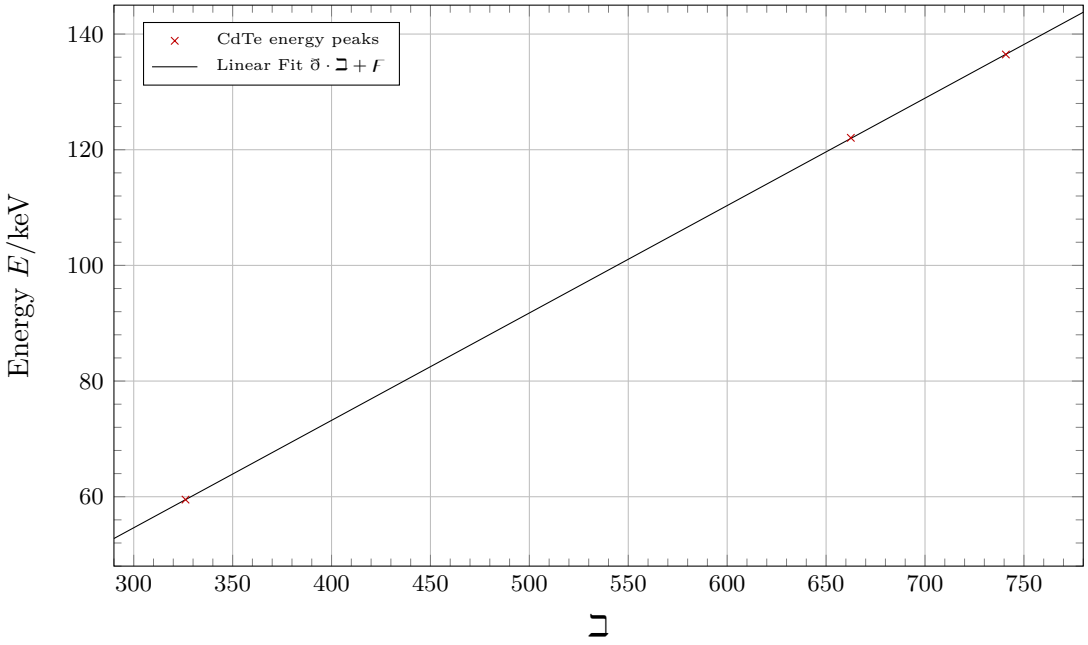


Figure 51: Linear regression in order to determine the energy conversion formula for CdTe.

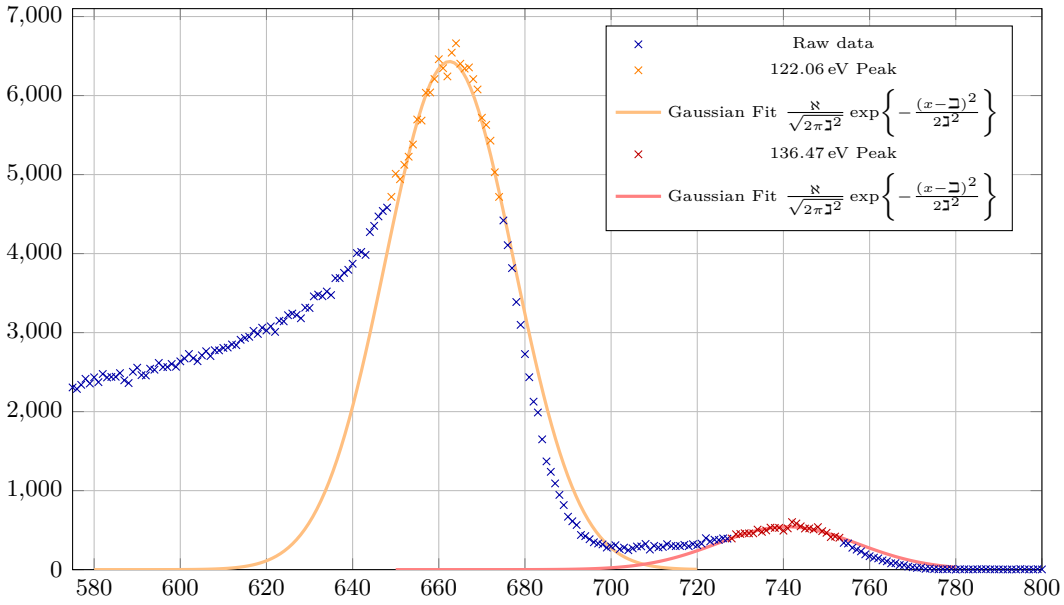


Figure 52: Background-subtracted counts of each MCA channel of the CdTe detector using the cobalt source. Additionally, both Gaussian fits of the peaks are shown.

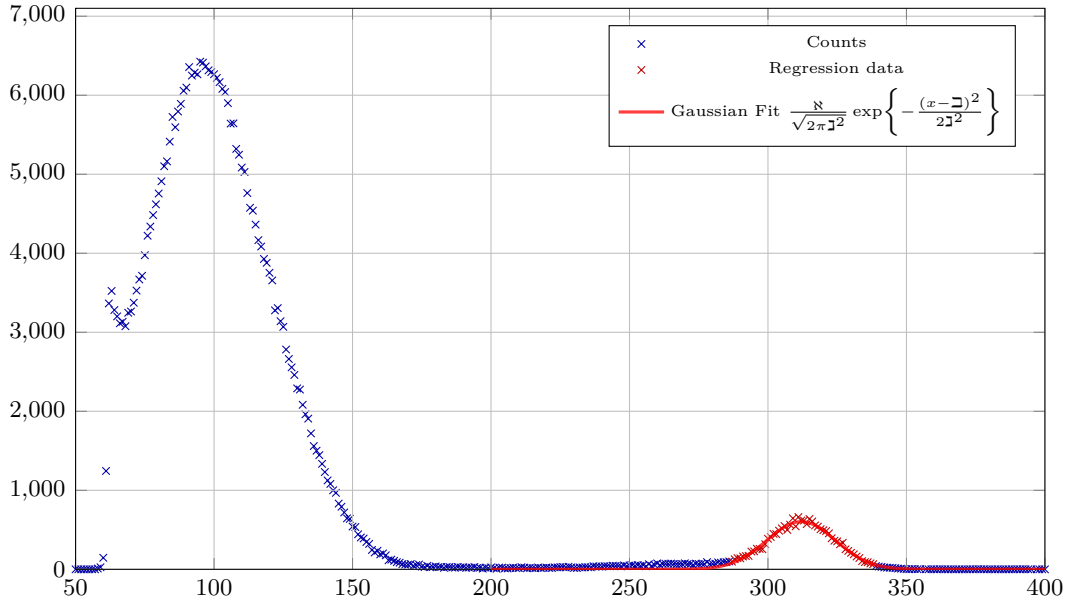


Figure 53: Background-subtracted counts of each MCA channel of the silicon diode using the cobalt source. Additionally, the Gaussian fit of the peak is shown.

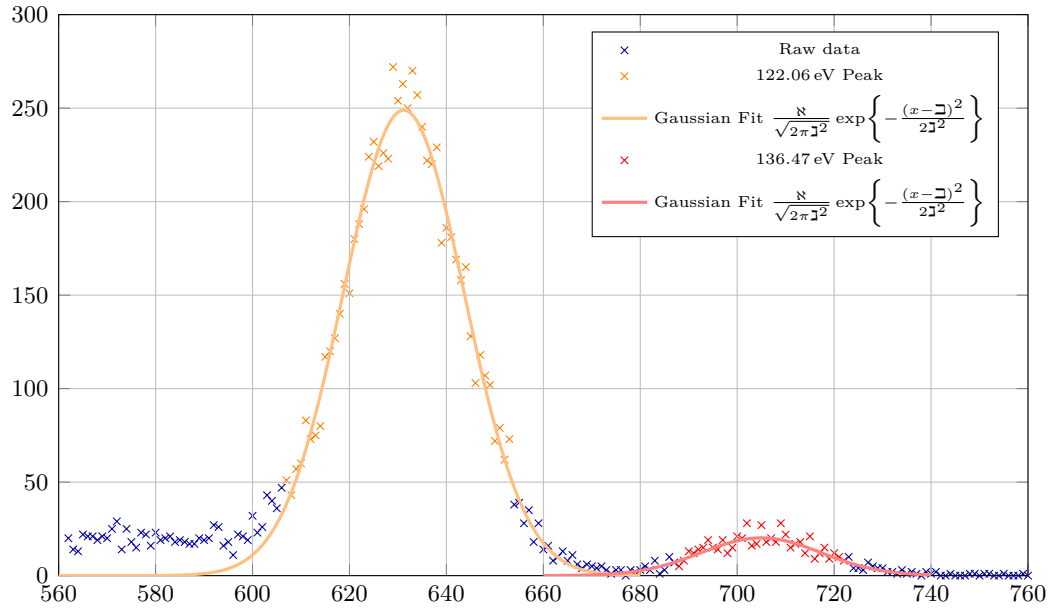


Figure 54: Background-subtracted counts of each MCA channel of the silicon diode using the cobalt source. Additionally, both Gaussian fits of the peaks are shown.

## A.2 Lab notes

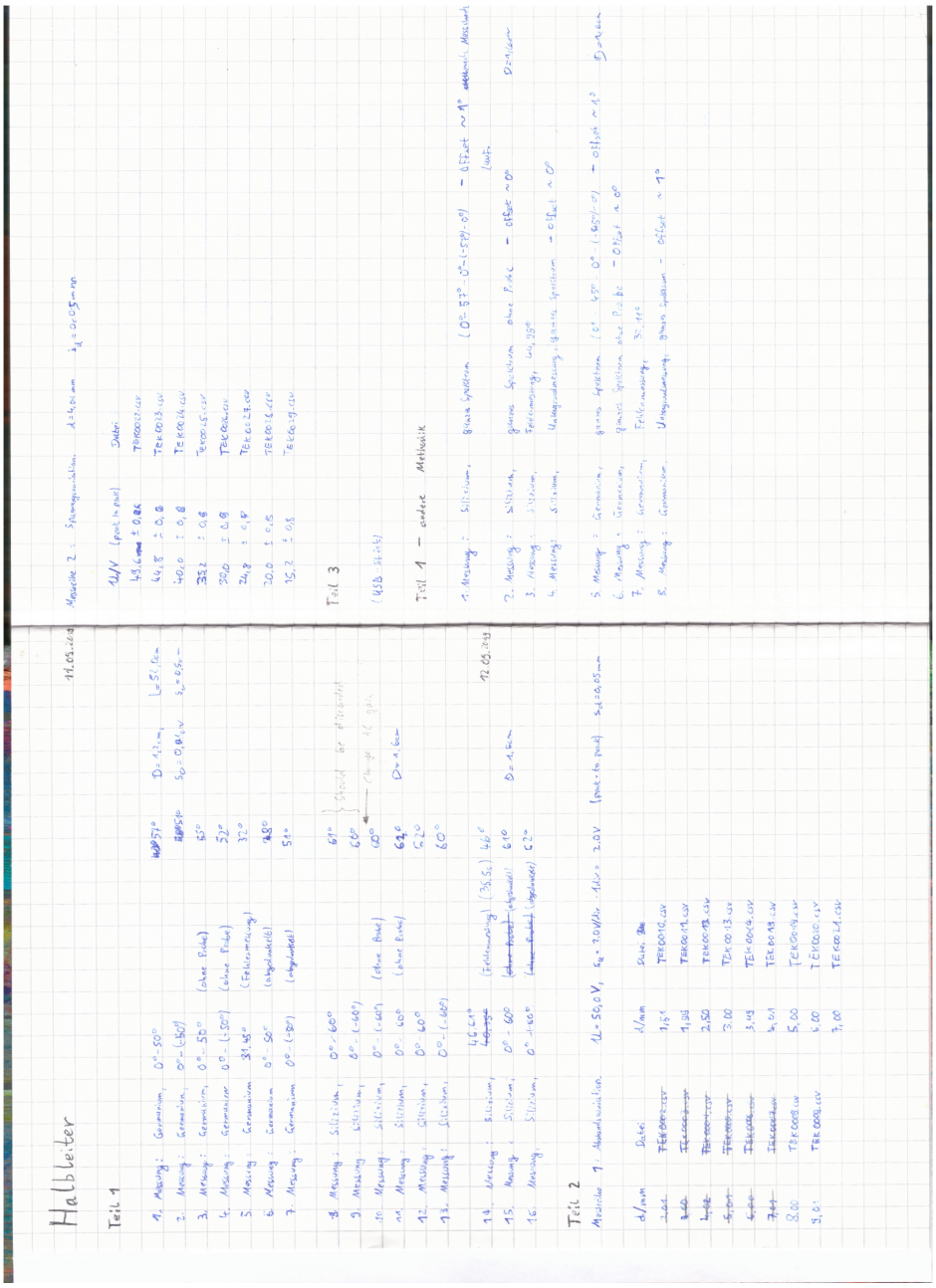

# List of Figures

## List of Tables

# Bibliography

[1] *CRC handbook of chemistry and physics*. Bd. B. 58. CRC Press, 1978

[2] Amrein, Simon: *Halbleiter und Halbleiterdetektoren*. 2008

[3] S. Amrein, K. Lohwasser, M. Kohli, S. Kuhn: *Versuchsanleitungen Fortgeschrittenen Praktikum Teil I - Halbleiter*. 2013

[4] Wang, F. F. Y.: *Introduction to Solid State Physics*. 1988. – 212–217 S.